A Study of Durability for Elastomeric Fuel Cell Seals and an Examination of Confinement Effects in Elastomeric Joints

Justin Klein

Thesis Submitted to the Faculty of the Virginia Polytechnic Institute and State University in Partial Fulfillment of the Requirements for the Degree of

Masters of Science

In

Engineering Mechanics

David A. Dillard – Chair

Scott W. Case

Robert B. Moore

May 4th 2010

Blacksburg, Virginia

Keywords: Elastomer, Degradation, Durability, Lifetime, Stress Relaxation, Strain Energy Release Rate, Confinement, Thermal Expansion, Varying Thickness

A Study of Viscoelastic Behavior on Durability and Confinement in Elastomers

Justin Klein

ABSTRACT

Proton exchange membrane fuel cells typically consist of stacks of membrane electrode assemblies sandwiched between bipolar plates, effectively combining the individual cells in series to achieve the desired voltage levels. Elastomeric gaskets are commonly used between each cell to insure that the reactant gases are isolated; any failure of a fuel cell gasket can cause the reactants to mix, which may lead to failure of the fuel cell. An investigation of the durability of these fuel cell seals was performed by using accelerated characterization methods. A hydrocarbon sealant was tested in five different environments to simulate fuel cell conditions. Viscoelastic properties of these seals were analyzed using momentary and relaxation compressive stress tests. Material properties such as secant modulus at 100% strain, tensile strength, and strain at failure were determined using dog-bone samples aged at several different imposed strains and aging times in environments of interest. Tearing energy was evaluated using trouser test samples tested under different rates and temperatures after various environmental aging conditions. Additionally, tearing tests were conducted on samples tested in liquid environment. A viscoelastic and mechanical property characterization of these elastomeric seals under accelerated aging conditions could help understand the behavior and predict durability in the presence of mechanical and environmental loading.

Additionally, the effects of confinement have been evaluated for a bonded joint with varying thickness along the bonded direction. The Dreaming project is a glass art project in

Fredrick, MD which incorporates such a varying thickness joint where thermal expansion of the adhesive has caused the glass adherend to break and debonding of the sealant. To examine this joint design, finite element analysis has been used to determine the effects of thermal expansion on such a complex geometry. Nine different test geometries have been evaluated to determine the effect of confinement coupled with thermal expansion on joint design with an elastomeric adhesive. Once evaluated, design changes were performed to try to reduce the loading while maintaining the general joint design. Results of this analysis can be used to determine the effects of confinement on a complex elastomeric joint.

Acknowledgements

I would like to thank my advisor Dr. David Dillard for all his support and encouragement. I have been honored to be able to work under an advisor who has such a passion for teaching and is extremely acknowledgeable. It has been such an rewarding experience, one that I will never forget.

I would also like to thank the members of my committee Dr. Scott Case and Dr. Robert Moore for their support and insight into this project.

I would like to thank Dr. Hitendra Singh and Gilles Divoux for their insight and vast contributions to this project.

I would like to thank UTC Power for supporting this research. I would specifically like to thank Jason Parsons at UTC Power as well as Dr. Yanbing Wang at Henkel and Mark Belchuk at Freudenberg- NOK for their encouragement and guidance throughout this project.

I would also like to thank my lab mates specifically Andy Borum, Katherine Finlay, Youliang Guan, Brad Miller, Katie Murray, Edoardo Nicoli, Kshitish Patankar, Chase Siuta, Geoffrey Tizard, and Lei Yan. I would also like to thank members of my previous lab, specifically Steve Anton, Onur Bilgen, Jacob Davidson, Kahlil Detrich, Andrew Duncan, Andy Sarles, Seyul Son, Josh Stenzler, and Pablo Tarazaga.

I would also like to thank Mellissa Nipper for her constant support.

I would also like to thank the Engineering Science and Mechanics Department at Virginia Tech.

I would also like to express my sincere thanks to my friends and family for their love and support. Specifically, my parents Ross and Diane Klein for their constant support and shaping me with the morals and drive that I have, which make me the person that I am today. Thank you.

Table of Contents

Table of Figures

List of Tables

Chapter 1: Introduction

1.1 Research Motivation

The motivation of this research is to investigate the material response of an elastomeric gasket used in a fuel cell application as well as to investigate the effects of confinement on a variable thickness joint. Alternative energy sources have become a large area of research as current energy sources are harmful to the environment and are rapidly depleting. One such area of research has been a proton exchange membrane fuel cell. These fuel cells contain an elastomeric gasket that must withstand the life of a fuel cell as any gasket degradation can impact the performance of the fuel cell. Gasket performance is controlled by the ability of the gasket to seal. This is impacted by any changes in sealing force or a crack causing failure in the gasket. For these reasons, the seal material is evaluated to determine momentary and relaxation properties as well as mechanical behavior and tearing energy as a function of aging.

The materials are aged in aggressive environments at elevated temperatures to mimic a fuel cell environment. Over a period of several months, the momentary and relaxed stiffness of a specific seal geometry was investigated while submerged in aggressive environments. Additionally, the material's mechanical behavior is evaluated for samples that have been strained and aged to determine the mechanical behavior change as a function of age. Furthermore, the tearing energy has been evaluated to determine the materials resistance to crack propagation. Tearing energy has been compared for as-received samples to aged samples. Additionally, tearing energies have been evaluated for samples tested in liquid environment to determine environmental effects on tearing. By understanding these various modes of failure for the fuel cell gasket this research can help improve the viability of this emerging alternative energy solution.

The effects of confinement have also been investigated for a variable thickness joint. The Dreaming project in Fredrick, MD incorporates such a joint in a glass art project where thermal expansion of an adhesive of varying thickness has caused the glass adherend to crack and the adhesive to delaminate from regions of the upper adherend. To understand these effects, a finite element model has been analyzed for various joint geometries. For this research, the effects of increasing the thickness change in the joint as well as increasing the confinement has been examined for nine different geometries. Additionally, design changes have been performed to limit the effects of thermal expansion as well as confinement. By understanding how varying the joint geometry as well as various design changes effects the load distribution of the joint, the effects of confinement can be analyzed.

1.2 Thesis Organization

This thesis was written in manuscript form with a focus on three different areas which are the topics of the three chapters to follow.

To begin, the first manuscript discusses the durability of an elastomeric material for fuel cell application. This chapter investigates the impact of momentary and relaxed stress states in an aggressive environment to evaluate seal behavior as a function of time. Additionally, this chapter examines the mechanical behavior of the seal material as a function of aging. This was performed by measuring the secant modulus at 100%, the tensile strength and the strain at failure on samples that have been strained and aged in aggressive environments at high temperatures.

The second manuscript investigates the impact of aging on tearing energy for a fuel cell gasket material. The effect of crack rate and temperature has been investigated in order to construct a tearing energy master curve. This master curve was compared for the as-received

samples to samples that have been aged. The tearing energy has also been evaluated for samples tested in a liquid environment.

The final manuscript examines the impact of confinement on an elastomeric joint of variable thickness. Through the use of finite element analysis via Abaqus, several joint geometries have been investigated to determine how a varying thickness adhesive coupled with confinement impacts joint performance. Additionally, the design of this joint has been altered to investigate design changes which could reduce the stresses induced in the adherends.

Chapter 2: Assessing Durability of Elastomers for Fuel Cell Application

2.1 Introduction

For a fuel cell environment, materials used undergo harsh environmental conditions which include acidic conditions as well as frequent temperature and humidity cycling. In a typical automotive fuel cell stack, there can be over 300 cells used to power a hydrogen car. Specifically for hydrogen powered vehicles, a proton exchange membrane (PEM) fuel cell consists of membrane electrode assemblies stacks sandwiched between bipolar plates. By effectively combining the individual cells in series, the desired voltage can be achieved. For this reaction to be efficient, the reactant gases, which alternate between the anode and cathode sides of each cell, must be prevented from mixing. This is often achieved through the use of elastomeric seals or gaskets in PEM fuel cells. Any gasket degradation or failure, during either operation or rest, can allow the reactants to mix with each other directly, which will impact the performance and operation of the fuel cell. For this reason, the durability of the elastomeric material is evaluated to examine the behavior of the fuel cell seal under accelerated aging conditions. For this study, material characterization of gaskets has been extended for testing seals which undergo aggressive conditions. Stress relaxation response has been used to determine seal performance and lifetime of seals used in various applications across a variety of industries. Specifically, the automotive industry specifies stress relaxation tests for critical sealing products [1]. The service life of seals depends primarily on the decay of compressive forces between the seal and its mating surface [2]. Furthermore, the material's mechanical properties as a function of aging play an important role in the life of these types of materials. Uniaxial tension testing has been used vastly in determining mechanical response of a given material system. In particular, the Young's modulus, tensile strength and ultimate strain can

provide insight into material behavior. Additionally, when coupled with accelerated aging, the materials response to degradation can be determined. For this reason, long term chemical and mechanical stability of the seals is necessary and is investigated here to determine lifetime predictions and behavior of the fuel cell seal material[3].

2.2 Background

Relaxation of elastomers may involve either physical or chemical relaxation or both. Physical relaxation of polymers involves the flow of chains past one another as well as the movement of entanglements. For elastomers, in the absence of chemical effects, the physical relaxation phenomenon is reversible upon the removal of the strain [2]. Chemical relaxation may consist of either scissioning of covalent bonds at crosslinks or along the backbone of the polymer or additional crosslinking [2, 4]. Chain scissioning of bonds can cause the effective crosslink density of the network and the equilibrium rubber elastic modulus to decrease with time [5]. Additional crosslinking can continue to occur in rubber materials, as some residual curing agent in the material may exist and can cause further curing in the sample, especially at elevated temperatures. In some cases, additional crosslinking can also occur due to the breaking and reforming of bonds in the material as seen in a dynamic network [1]. In elastomeric components when temperature and/or deformation are large, chain scissioning of crosslinks and possibly in-situ re-crosslinking can result in time dependent softening (relaxation) [6]. For idealized stress relaxation behavior in gaskets, after the initial physical relaxation of the polymer chain, the chemical relaxation process is minimal in comparison to the physical, and the sealing force is steady and constant as a function of aging [7]. It can be seen that measuring the stress of a material at constant temperature and strain in a degrading rubber network provides a measurement of the crosslink density as a function of time. However, this measure of crosslink density is only of the load bearing chains, if the degradation involves additional crosslinking as well as chain scissioning, the new crosslinks formed are generally

assumed not to be load bearing [8]. Tobolsky recognized this fact and determined that the permanent set in a material, which is a measure of a sample's permanent deformed shape after relaxation, can be correlated to stress relaxation under continuous strain and the momentary stress response [9]. Stress relaxation tests, which hold a sample at a prescribed strain continuously, monitor only the load bearing chains. Any new chains formed contribute little to the stress state; therefore the force relaxation characterized by this test represents a combination of the chains that have undergone scissioning as well as the viscoelastic relaxation at that specific time. A measure of the momentary stress response, which stretches a sample to a prescribed strain then releases it to its initial condition, can provide a measure of the crosslink density of the sum of the original remaining network and the new network formed during degradation at a given time. Momentary loading measurements of the stiffness are conducted by loading a specimen held in the same environment for a brief instant to a set compression length and quickly returning the specimen to its original strain condition. By measuring both momentary stiffness and stress relaxation response, the net rate of scissioning and crosslinking in the sample can be determined [9]. If the degradation involves only chain scissioning and no new networks are formed, both the momentary stiffness and stress relaxation response tests will measure the same crosslink density [8].

By monitoring the rate of relaxation with respect to temperature, lifetime predictions can be made using an Arrhenius approach assuming that the failure process consists of chemical reactions where the rate of reaction increases with temperature [7]. The Arrhenius model is generally used when thermo-oxidative aging mechanisms are dominant. This approach assumes that the chemical degradation process is controlled by a reaction rate. If one plots the log of the reaction rate versus the reciprocal of temperature, a straight line behavior is expected and allows for simple extrapolations to various temperatures if the Arrhenius approach is valid for the temperature of interest. This method was employed by Ronan for testing stress

relaxation in elastomers where he compared the Arrhenius plot obtained from compressive stress relaxation at elevated temperatures in air to the shifts determined from dynamic mechanical analysis and determined them to be in good agreement with each other [1].

In addition to the stress relaxation characterization, uniaxial tension tests can be used to characterize the mechanical behavior of a material. Generally, as polymers age they tend to become more brittle and this could affect any long-term application of the material [10]. Analysis of the mechanical behavior, such as elastic modulus, tensile strength and strain measured at various aging times and conditions, is important to developing an understanding for materials that require reliability and or durability in their applications [11]. The aging characteristics of a material can be evaluated as a function of time, environment and strain by prescribing strain on samples subject to various environments and temperatures. Material samples held at different strains in environment could be subjected to additional crosslinking or chain scissioning, which could affect the material properties. Additionally, failure from environment could occur due to chemical interactions affecting the composition of the material and its physical properties as the environment can cause chemical bonds to break and/or reform [12]. Since a material's durability is a function of mechanical behavior, the material's mechanical response will be evaluated in terms of stress relaxation and uniaxial tension to determine the durability of this material.

2.3 Experiment

An examination of the durability of fuel cell seals has been conducted to determine the effects of accelerated aging on elastomeric materials designed for fuel cell applications. Two different types of experiments have been carried out to determine the various mechanical properties of these materials specifically stress relaxation and uniaxial tension. Additionally, tearing energy as a function of durability has also been evaluated and is examined in Chapter 3.

Stress relaxation tests have been used to characterize long term durability in accelerated aging conditions. Stress relaxation was chosen because the application for the material tested is sealing and a comprehensive understanding of stress relaxation over time could provide insight into the materials sealing force as a function of aging. Since the geometry tested under these relaxation conditions is complex, the stress will not be directly calculated instead, the relaxation effects will be correlated to force as a function of time. Uniaxial tension tests have been performed to determine the mechanical behavior of these materials in aggressive environments and to provide insight into the material's response as a function of aging.

Materials

The material tested was a hydrocarbon elastomer developed and provided by Henkel Corporation (Rocky Hill, CT). This heat cure material system was cured by heating in a molding tool at 120°C for two to three minutes for sufficient crosslinking to occur for mold removal and then post cured at 130°C for one hour by Freudenberg-NOK (Plymouth, MI). Sheets of 200 mm x 200 mm x 0.5 mm thick samples of pure elastomer were molded for uniaxial tension samples. Sub-scale molded o-rings seals (SMORS), a scaled down version of the full sized part to be used in the membrane electrode assembly, were molded onto 40.5mm diameter disks of 0.356 mm thick gas diffusion layer. In the full size part, the elastomeric gasket will be molded with the membrane electrode assembly in the center of the elastomeric gasket; however for the SMORS tested here; the center of the seal consists of only the gas diffusion layer. These SMORS, seen in Figure 1, are used for stress relaxation tests as they are the geometry that will be used for sealing in the fuel cell and an understanding of the relaxation behavior on the specific geometry used will provide better insight into the actual behavior of these seals in a fuel cell.

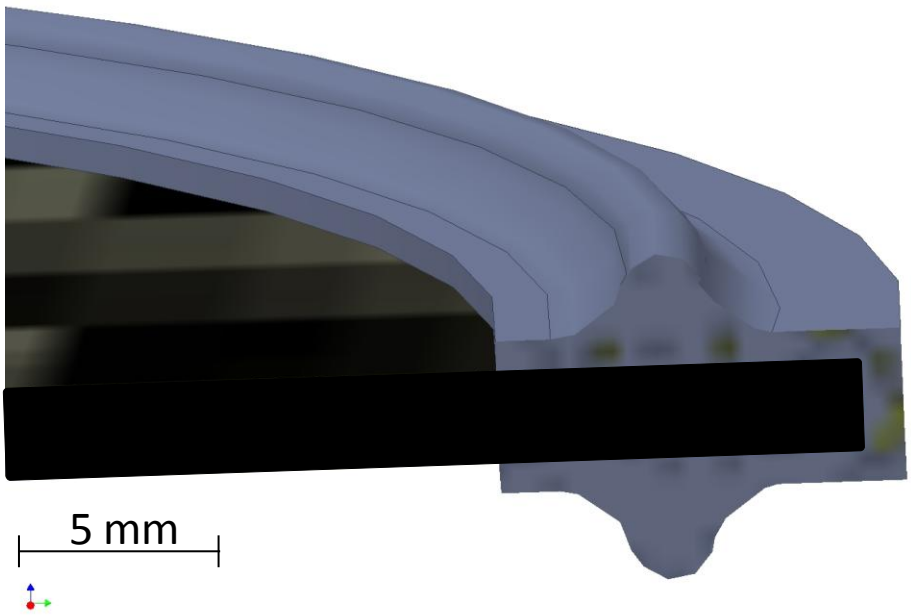

Figure 1: Cross-sectional view of a portion of sub-scale molded o-ring (SMORS) [13]

2.3.1) Compressive Stress Relaxation Fixtures

For this experiment, two different fixtures were used to examine the momentary stiffness and relaxation behavior separately. Both fixtures are similar to each other; the only difference is that the continuous fixture has been outfitted with a load cell to measure relaxation at short sampling intervals programmed by the software. The intermittent fixture was designed for testing in a load frame, thus limiting data collection to times when the fixtures were removed from the oven and placed in the test frame for evaluation. The fixtures were made entirely of 316 stainless steel to reduce corrosion in aggressive environments at elevated temperatures.

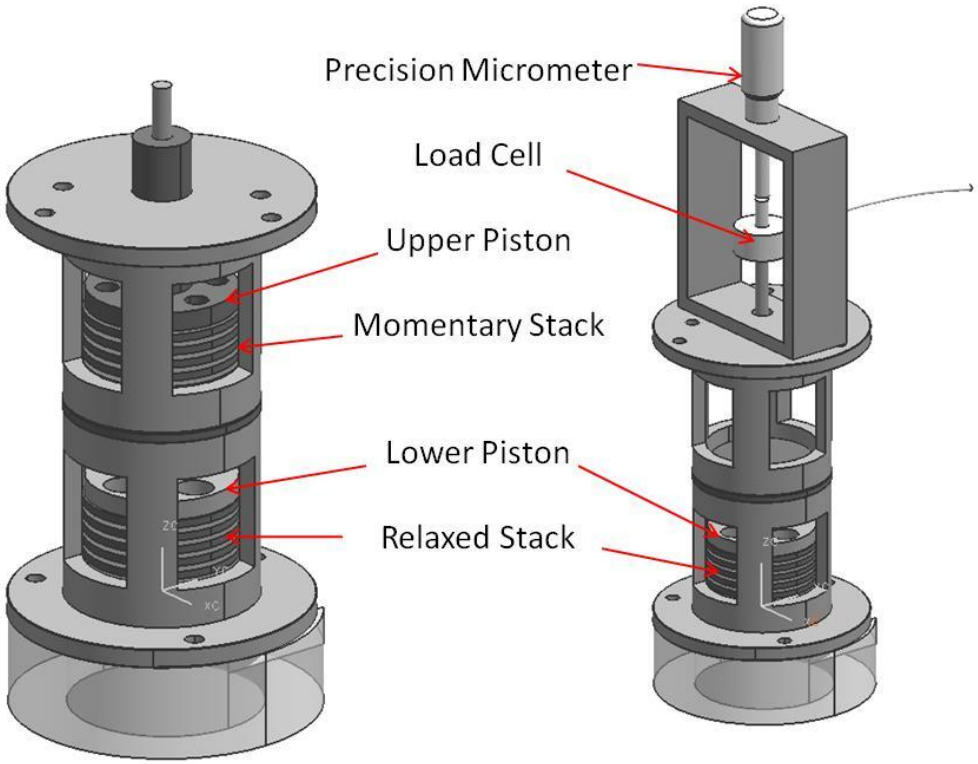

Figure 2: Intermittent (left) and continuous (right) stress relaxation fixtures [13]

As seen in Figure 2, the continuous stress relaxation fixture, used to measure the relaxed state of stress, contains a load cell (Interface WMC-25,Scottsdale, Arizona). This load cell was chosen to provide accurate force measurements for small loads under humid conditions as the samples are immersed in aggressive environments at high temperatures. The load cell is environmentally sealed through the use of the epoxy gasket around the stem of the load cell to insure the environmental and temperature conditions of the test do not affect the recorded load. The load cell is mounted onto the relaxation fixture through the lower plunger; the top stem of the load cell is loaded by a high precision micrometer with a resolution of 0.08 mm. The micrometer is attached to the fixture in the upper bracket and is used to accurately impose a desired compressive displacement on the samples. The intermittent stress relaxation fixture does not contain a measuring device instead the displacement is fixed through use of a 1.5 mm thick washer that imposed the desired compression. This fixture was designed around testing the momentary stiffness as well as stress relaxation simultaneously through the use of

two chambers, an upper and a lower. The upper chamber is used to probe the momentary response of a stack of SMORS that is not loaded during the exposure, but are strained briefly to determine the momentary response and are then returned to their original state. The lower chamber maintains a given compression in the lower samples during environmental exposure by imposing a displacement with the use of a spacer. The lower chamber holds the prescribed strain; by varying the thickness of the spacer different compression levels can be set. This chamber when tested in a load frame measures the relaxation stiffness as a function of time. Both fixtures are placed on a polycarbonate base to allow them to rest on a flat surface. This is needed because the loading rod, which prescribes the desired strain on the lower stack through use of a spacer, protrudes from the base of the fixture. These fixtures are placed in glass containers filled with the liquid environment and then covered with a clamped glass lid to prevent evaporation and contamination.

2.3.2) Stress Relaxation Experiment Preparation

The samples tested in this fixture are a stack of five SMORS arranged between parallel 316 stainless steel washers centered about the loading piston. The stack configuration was utilized to provide a better strain resolution during compression as individual SMORS consist of only 1.5 mm of elastomeric material. By arranging five specimens in series, the strain resolution of the test increases as in order to achieve 20% compression, the stack is compressed 1.5 mm as opposed to 0.3 mm for an individual sample stack. For the continuous fixture, only the lower chamber contains samples as this fixture only measures the force relaxation of the specimen stack. For the intermittent fixture both the upper and lower chambers contain samples as this fixture tests both the momentary stiffness as well as the stress relaxation. The mechanical properties of the SMORS were examined in five different environments: 120°C air, 90°C air, 90°C deionized (DI) water, 90°C 50/50 ethylene glycol, and 90°C 0.1 M sulfuric acid solutions. The intermittent stress relaxation fixtures for testing in liquid environment were placed in glass

containers, the environment was added, a glass lid was placed on top of the fixture and then the fixtures were placed in a gravity convection oven for environmental exposure. Those tested under air-aging were placed directly in the oven. The continuous stress relaxation fixtures were placed in individual glass containers into which the desired environment was then added. The chambers were then sealed using a room temperature cure silicone to prevent evaporation and the fixtures were placed in a water bath at 90°C. The continuous stress fixtures were individually sealed due to the height addition from the micrometer and load cell, seen in Figure 2, which prevents the use of a flat lid. The addition of these components caused the overall height of the continuous fixture to be more than the height of the glass container so to minimize evaporation of environment; a room temperature cure silicone was applied between the exterior edges of the continuous fixture and the interior wall of the glass jar. A water bath was used to maintain the desired environmental temperature of the SMORS in the continuous fixture, to prevent direct heating of the load cells as well as the leads connecting the load cell to the data acquisition system. Since the continuous stress relaxation fixtures were heated in a water bath, additional insulation was added to the glass container and the top of the water bath. As illustrated in Figure 3, a PMMA box was added over the water bath to maintain a consistent temperature in the samples and to limit the impact of the laboratory's atmosphere on this sensitive test.

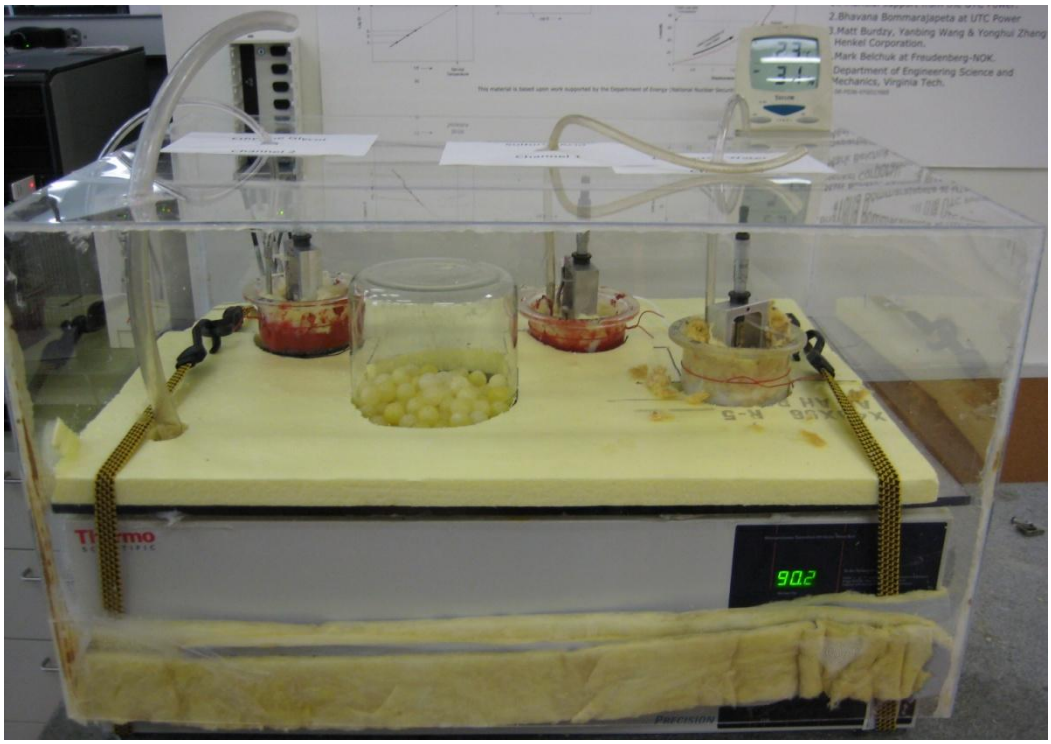

Figure 3: Continuous stress relaxation experimental set-up

All samples were allowed to equilibrate in their environment and temperature for a week under no loading before testing. This extensive equilibrium time is used to insure that the samples relaxation behavior is uniform. Relaxation has been measured for this system for shorter equilibrium times; however the results exhibited erratic behavior uncharacteristic of relaxation. For this reason, a longer equilibrium time was used as results from this equilibrium time show stable behavior.

2.3.3) Uniaxial Tension Experiment Preparation

Uniaxial tension samples were cut out of 0.5 mm sample sheets using an ASTM D412 Die C and a clicker press (Qualitest Inc., Buffalo, New York). The sample ends were reinforced with 20 mm of tape (SA, China) placed on both sides at the top and bottom of the dogbone samples and holes were punched in the sample to hold the sample under prescribed strain conditions in a custom made fixture shown in Figure 4.

Figure 4: Image of dogbone sample

Since these samples are held in strain for long periods of time, the stress concentrations from the pins cause the samples to tear unless the samples are reinforced. In fact, it was found that the stress concentration from the holes causes the samples to break in air at room temperature after a very short period of time (2-3 days). Since these samples will be held at elevated temperatures for long periods of time, over 2700 hours, the samples were reinforced. The tape is assumed be perfectly bonded for the duration of aging and is assumed to have a constant stiffness as a function of time. The custom built screening fixture was used to hold strain on the samples in environment over long periods of time to provide for accelerated aging. The fixture, seen in Figure 5, was made of 316 stainless steel to prevent corrosion in aggressive environments. Additionally, holes were drilled into each side at various spacing to allow for different strains to be prescribed on the samples.

Figure 5: Custom built screening fixture used to prescribe held strain on samples

The samples were placed on the screening fixture at three different nominal strain levels (0, 25, and 50 % strain). These strains were presented in a previous student's work where the strain was determined to be 0, 22.14% and 49.18% from a finite element model that considers the taped region to be perfectly bonded [13]. These strains are in good agreement with the strain recorded from the laser extensometer of 0, 22% and 49% and will be reported as 0, 25 and 50% strain as an approximation to the actual strain. For samples tested in a liquid environment, the screening fixture was placed in a glass container, the desired liquid environment was added, a glass lid was added to prevent evaporation, and the loaded fixture was then placed in a gravity convection oven at 90°C to allow the specimens to age. The environments used were deionized (DI) water, 50/50 ethylene glycol, and 0.1 M sulfuric acid. For air-aged samples, the screening fixture was placed directly in the oven at 90°C. All samples were aged for four different aging times: 2 weeks, 4 weeks, 8 weeks, and 16 weeks and compared to the as-received material.

2.3.4) Stress Relaxation Test Procedure

The continuous stress relaxation fixture was displaced to 20% compression by using the precision micrometer mounted above the stack. The load was recorded with a 110 Newton Interface WMC-25 load cell connected to a data acquisition system. A custom designed LabView (National Instruments, Austin, TX) code running on a dedicated computer recorded the load measured over the extent of the experiment. The intermittent fixture was removed from the oven to measure the mechanical properties of the samples periodically and then replaced in the oven to continue the aging process. The intermittent fixture was measured by placing the fixture into an Instron MicroTester 5848 load frame with an auto-calibrated 50 N capacity load cell. The load frame measures the force on the upper and lower stacks and the displacement is recorded from a built-in linear variable differential transformer used to measure the linear displacement of the load frame. By loading the upper and lower pistons separately, the stiffness can be measured over time for the momentary and relaxation states. The upper piston was loaded to a displacement equivalent to 20% compression on the SMORS. Since the lower stack is held in compression, loading the lower piston initially removes contact from the spacer. The point in which the contact from the spacer is completely removed represents loading of the lower stack's SMORS. At the transition point, the slope of the line changes from the loading curve from contact with the spacer to the loading curve of the samples in compression, it is this point which represents the load necessary to hold the material at the prescribed compression and is taken to be the relaxed stiffness. This is calculated by creating linear fits of the two lines and determining their intersection point. Figure 6 illustrates a comparison of the momentary and relaxed stress loading curves. Measurements were taken at a loading rate of 8 mm/min.

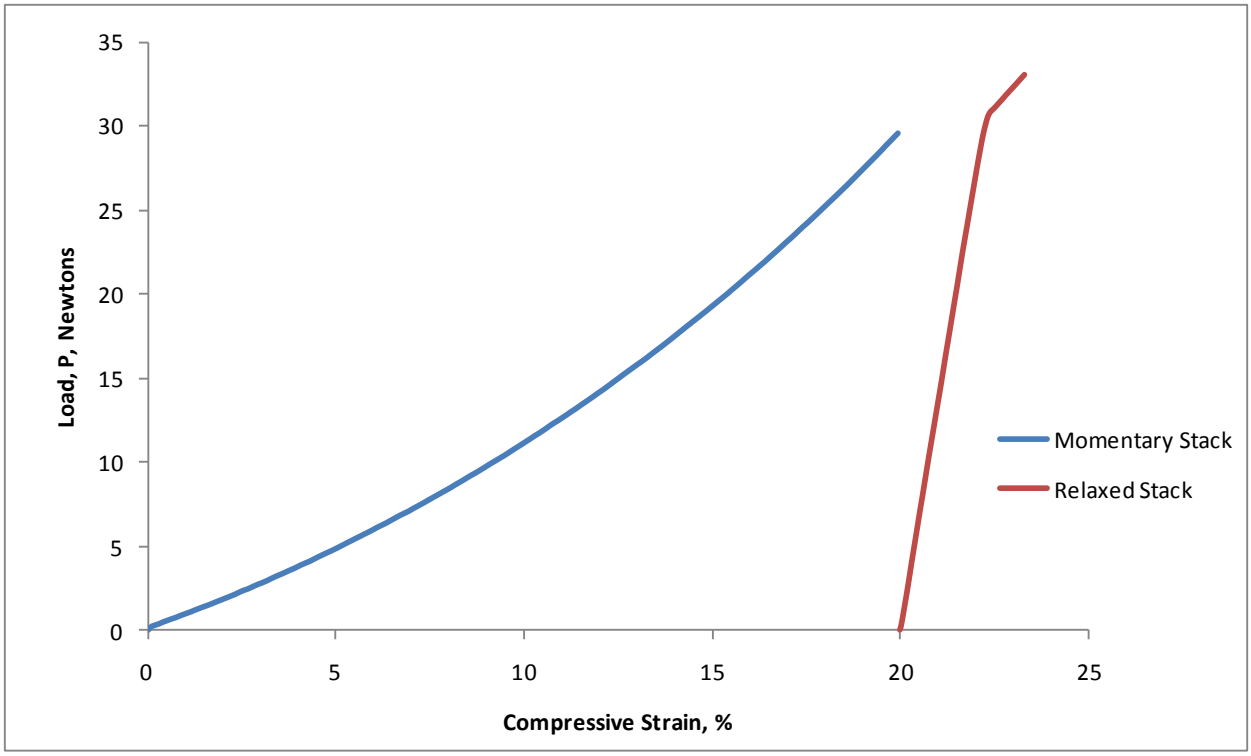

Figure 6: Relaxation Results of 120°C air-aged after one day in the intermittent fixture

2.3.5) Uniaxial Tension Test Procedure

After the samples had reached the desired aging time, they were removed from the screening fixture and cooled to room temperature. Reflective tape markers were placed on the specimen so that a scanning laser extensometer (Fiedler Optoelektronick, GmbH) could be utilized to measure the strain of the specimens without contact. Uniaxial tension tests were performed following the ASTM D412 standard using an Instron 5867 with a 100 N load cell. The samples were gripped using pneumatic compression grips and loaded to failure with a displacement rate of 500 mm/min at room temperature

2.4 Results and Discussion

For each aging environment in the intermittent fixture, load versus strain plots over prolonged times were used to create stress relaxation plots. The decay of the sealing force is

represented by $\frac{F(t)}{F_0}$, where F(t) is the force at a given time and F_0 is the initial force at the prescribed compression. The decay of force was plotted against time for both the momentary and relaxed states. For the intermittent fixture, the initial force is taken to be the first time the samples were tested in the load frame. For the continuous fixture, load as a function of time is measured continuously for each environment and then later normalized by F_0 where F_0 is taken a minute after initial loading. The difference in the initial relaxation load between the continuous and momentary fixtures may cause the differences in the results when compared to one another, however this difference is a function of how the fixtures are designed. The continuous fixture is designed to record all values of load for all time. The F_0 for the continuous fixture was recorded after one minute from loading. For relaxation tests that are ramp loaded, t_0 is generally assumed to be five times longer than the loading time. For the continuous fixture, one minute was used for this criterion as it took approximately 10-12 seconds to load the samples manually with the micrometer. The relaxed stack in the intermittent fixture is loaded before testing in the Instron through the use of a spacer. By the time the value is recorded in the load frame, which is approximately 2 minutes after the spacer has been loaded which took approximately 3-5 seconds; the samples had been loaded for longer than five times the loading time so this measurement is taken to be the initial force. The difference in measuring the initial restoring force could account for difference in the results as a large portion of the relaxation takes place soon after loading. Because of this, the intermittent fixture should measure a smaller decay in force in comparison to the continuous fixture. For each uniaxial tension test, load versus displacement is recorded. Engineering stress is calculated from the original cross-sectional area and strain is calculated from the laser extensometer and crosshead displacement. Ultimate strength and strain are reported as well as the modulus at 100% extension.

2.4.1) Intermediate Fixture Resolution Results

The resolution of this experiment has been determined by testing the same sample multiple times over the course of one day as seen in Figure 7.

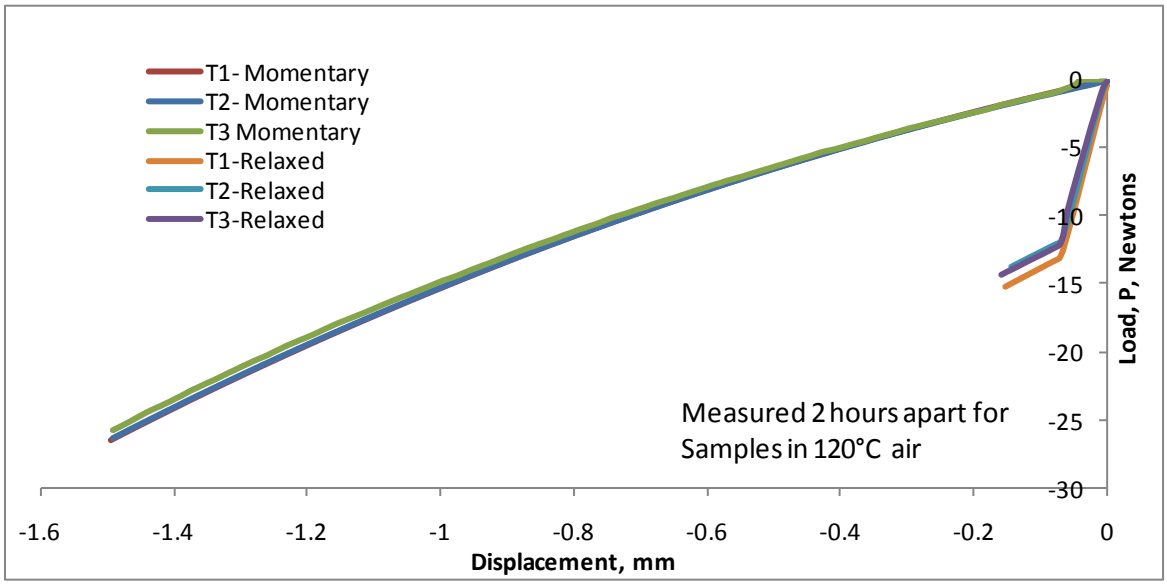

Figure 7: Measurement of resolution of the intermittent CSR

It can be seen here that the fixture shows little change for the momentary stiffness over the course of the test. The relaxed stiffness recorded over three different measurement times' shows slightly more variation in comparison to the momentary stiffness, however this test is a comparison of just one point so an average of the relaxed stiffness is a better approximation of the actual value. To do this, tests are conducted in rapid succession and the data presented for the momentary and relaxed states are an average of three runs.

Trial #	Momentary (N)	Momentary StDev	Relaxed (N)	Relaxed Stdev
1	26.51	0.072	13.33	0.46
2	26.33	0.072	12.42	0.64
3	25.79	0.087	12.00	0.31

Table 1: Comparison of the results from the intermittent CSR run over one day

These values have been compared for both the momentary and relaxed stack as well as the standard deviation across one succession of tests seen in Table 1. This figures show that while there is some variation between testing, the differences are small and across a given test there is little deviation. Furthermore, the standard deviation of one test is so small that any error bars shown on the graphs are not visible.

2.4.2) Momentary Stress Response Results

For momentary stress response, the change of load versus time illustrates a measure of the net rate of crosslinking and chain scissioning [9]. If no force decay is seen over time, the rate of crosslinking and chain scissioning is equal to each other or both are non-existent. Figure 8 illustrates that for SMORS aged in liquid environments, there is little to no change in the normalized load as a function of time.

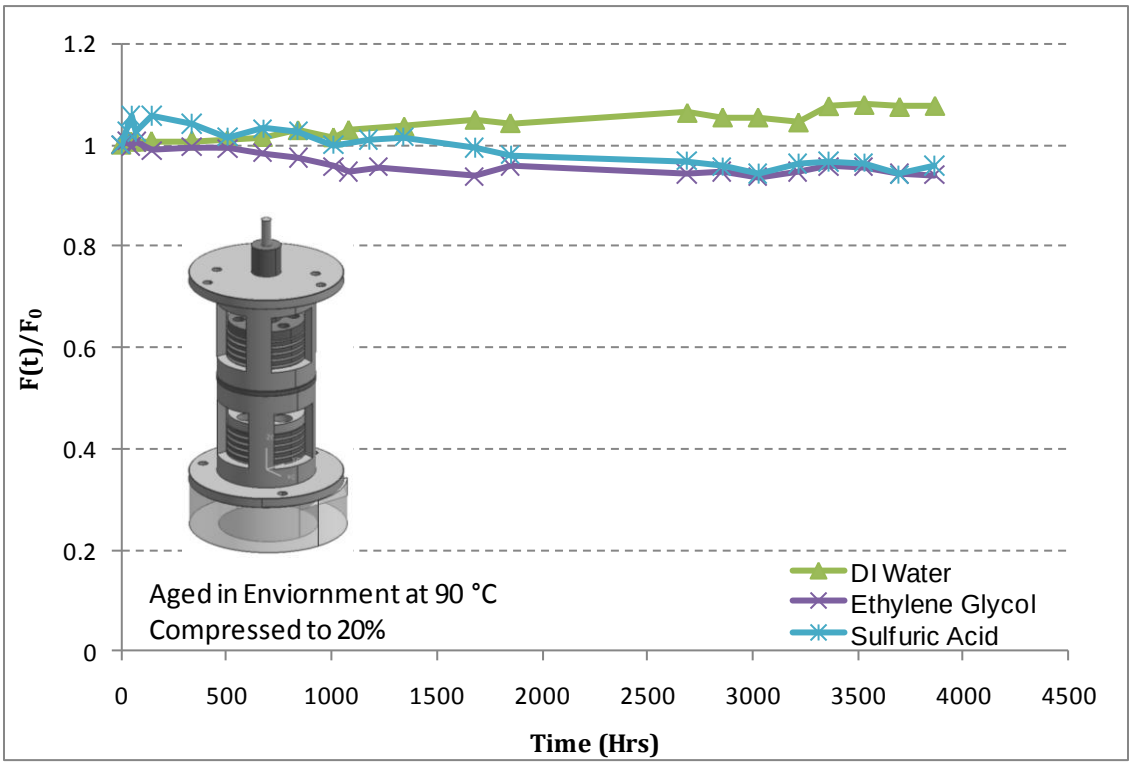

Figure 8: Momentary stress response in environment from intermittent fixture

After approximately 1000 hours, the deionized water samples show a slight increase in normalized load of approximately 8%. This increase in $\frac{F(t)}{F_0}$ suggests chemical effects of aging in the form of additional crosslinks being formed. It can be seen from Figure 8 that the decrease in momentary response for ethylene glycol and sulfuric acid occurs after over 500 hours of aging. This decrease in response denotes chemical effects of aging as significant physical aging effects that contribute significantly to stress relaxation happen on a shorter time scale [1-2, 14]. These crosslinks could come from the bonds breaking and reforming in this environment, or additional curing residue being present in these samples. Since these samples are submerged in liquid, an increase in oxygen causing additional crosslinking is unlikely, although this effect can be seen below in the air-aged samples, which exhibit a substantial momentary increase likely associated with an increase of crosslinks. One reason for this increase in crosslink density for deionized water aged samples could be that these samples undergo less chain scissioning in relation to additional crosslinking in comparison to the other environments which would increase the crosslink density of deionized water samples. If this is the case, additional crosslinking could occur from residual curing agents in the samples that are not broken due to the chemical effects of the environment. For both ethylene glycol and sulfuric acid specimens, momentary response show a slight drop in load of approximately 4%, illustrating that the rate of chain scissioning is slightly higher than that of additional crosslinking, which would explain the drop in sealing force. Some of the decrease in stiffness can be attributed to momentary sample relaxation, where the polymer chains achieve a new equilibrium status in response to periodic strain.

Momentary stress response tests conducted in air illustrate an increase in the stiffness of these materials as a function of time, as seen in Figure 9 .

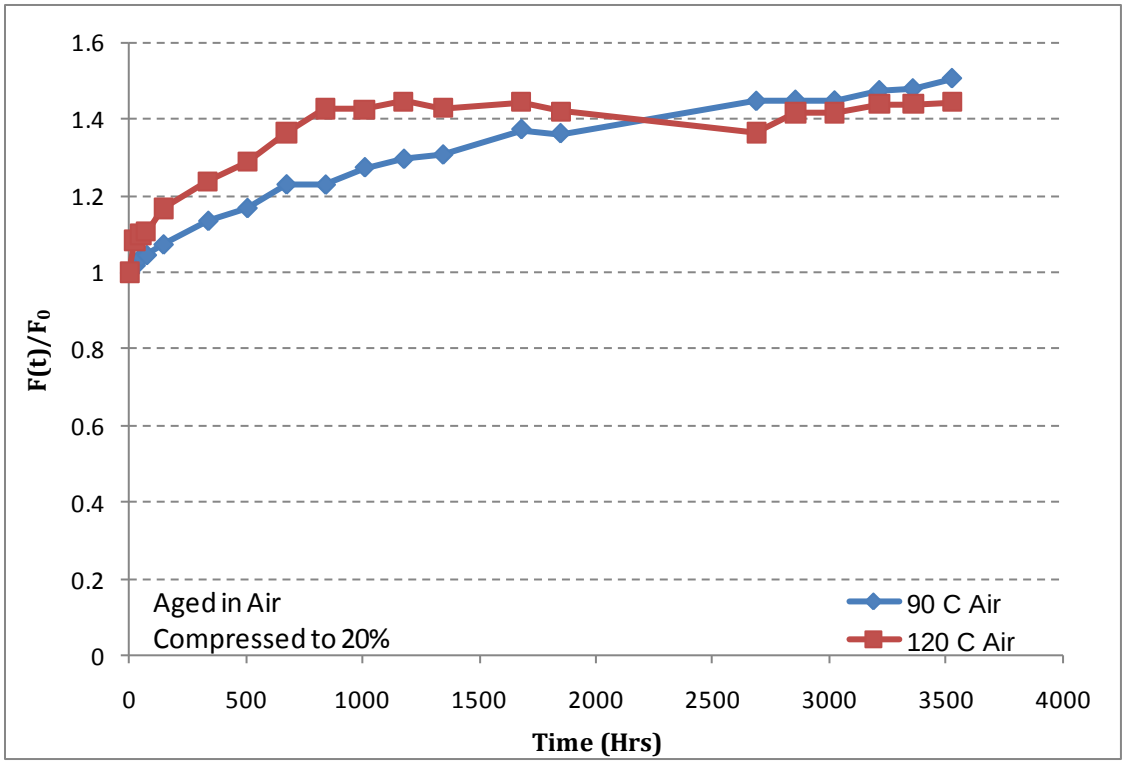

Figure 9: Momentary stress response in air from intermittent fixture

This increase in the stiffness suggests a large increase in crosslink density. Also, in general, as polymers age modulus increases and they can become more brittle [15]. Since the increase of the sealing force occurs over a long period of time frame (over 1000 hours), chemical effects are assumed to dominate [1-2].

It can also be seen that the degree of crosslinking is dependent on temperature. . In Ronan's work, applying an Arrhenius fit to compressive stress relaxation for elastomeric seals tested showed a good comparison to the shifts determined from dynamic mechanical analysis [1]. For this reason the Arrhenius fit has been determined for the seals tested in this work, however, since only two temperatures were tested it is unclear if this system follows Arrhenius behavior. The Arrhenius equation assumes that the degradation process is controlled by reaction rate k as seen in Equation 1

$$k = Ae^{\frac{-E_a}{RT}}$$

Equation 1: Arrhenius equation

where k is the reaction rate, A is the pre-exponential factor, E_a is the Arrhenius activation energy, R is the gas constant (8.314 J/mol-K), and T is the absolute temperature [15]. By computing the slope of the time it takes to reach equilibrium of the chemical reaction for the momentary stress response in air, we can determine the reaction rate for both 90 °C and 120 °C as 1.72 $x10^{-4}$ rate of decay/time and 4.47 $x10^{-4}$ rate of decay/time respectively. Plotting the natural log of the reaction rate verses the inverse of absolute temperature as seen in Figure 10 we can determine the Arrhenius activation energy.

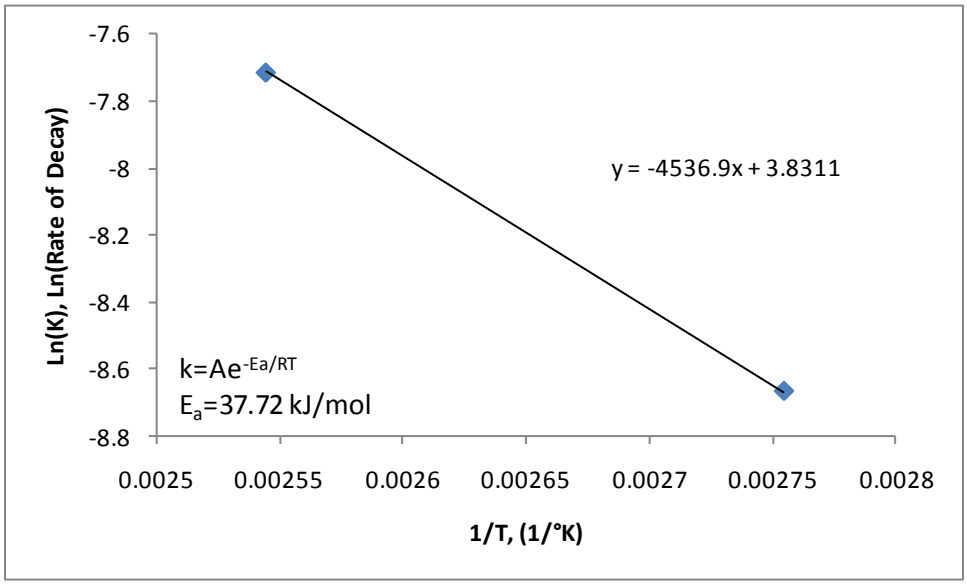

Figure 10: Plot to determine the Arrhenius activation energy

By taking the natural log of the Arrhenius equation as seen in Equation 2, we can determine a linear fit to the Arrhenius equation where the slope is equivalent to the Arrhenius activation energy over the gas constant.

$$\ln k = \ln A - \frac{E_a}{R}\left(\frac{1}{T}\right)$$

Equation 2: Linear fit to Arrhenius equation

Since only two different temperature tests were conducted it is not conclusive that this reaction is governed by Arrhenius behavior, however, when carried out for these two temperatures an activation energy of 38 kJ/mol was determined. This result is consistent with Gillen where for butyl rubber, higher temperatures reduced the expected activation energy for oxidation processes (from ~80 to 120 kJ/mol to ~38 to 56 kJ/mol) [14]. The low activation energy suggests the presence of diffusion limited oxidation. This effect is present when the rate of oxidation uses up dissolved oxygen faster than it can be replenished by diffusion from the surrounding atmosphere [2, 14].

For the momentary stress response in air, it can be seen that increasing the temperature increases the rate of which the material degrades. For samples tested in air, the momentary stiffness approaches a plateau value of $\frac{F(t)}{F_0} \approx 1.45$. Furthermore, it can be seen that after approximately 2700 hours, the stress response in 90°C air shows a plateau value very similar to that of 120°C. The fact that the plateau value is reached at a later time for samples aged in air at 90°C when compared to those aged in air at 120 °C is expected as the rate of the chemical reaction is faster at an increased temperature.

2.4.3) Relaxation Results

Relaxation measurements were obtained through two different testing fixtures, intermittent and continuous. Relaxation tests isolate the scissioning reactions in a sample. The decay of load is the direct measure of the physical relaxation of the material coupled with any scissioning of the polymer's molecular chains. Any new network formed (additional

crosslinking) in the relaxed state have little impact on the stress state as these networks are in equilibrium in the stretched sample. When the strain is removed from these samples, the new network formed has a direct impact on any compression set or permanent deformation seen in the sample [9]. The continuous fixture allows for all loads to be recorded as there is the force is recorded while the load is applied. For the intermittent fixture, the compressive displacement is prescribed and then the load is measured separately. The disadvantage of intermittent stress relaxation measurements is the initial loading point where most of the physical relaxation takes place is hard to determine as load is not measured continuously. Figure 11 illustrates the stress relaxation results from the intermittent fixture.

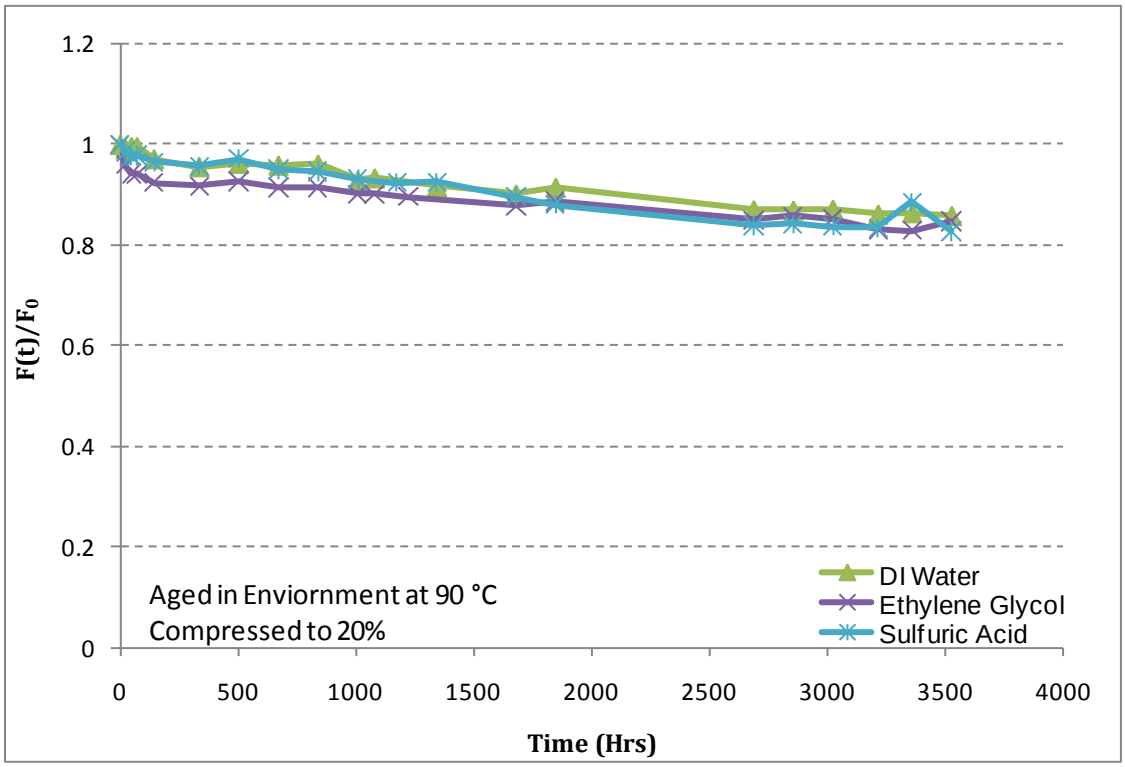

Figure 11: Stress relaxation in environment from intermittent fixture

It can be seen from Figure 11 that stress relaxation has an effect on the samples aged in environment more so than momentary stress relaxation. These samples show an average decay in sealing force of 16% after over 3500 hours. It can also be seen from stress relaxation

that after a long period of time the changes in the relaxed stiffness are minimal , indicating that chemical degradation past this point has a minimal effect on the elastomer [7]. The relaxation of liquid samples from the continuous fixture has also been measured in Figure 12.

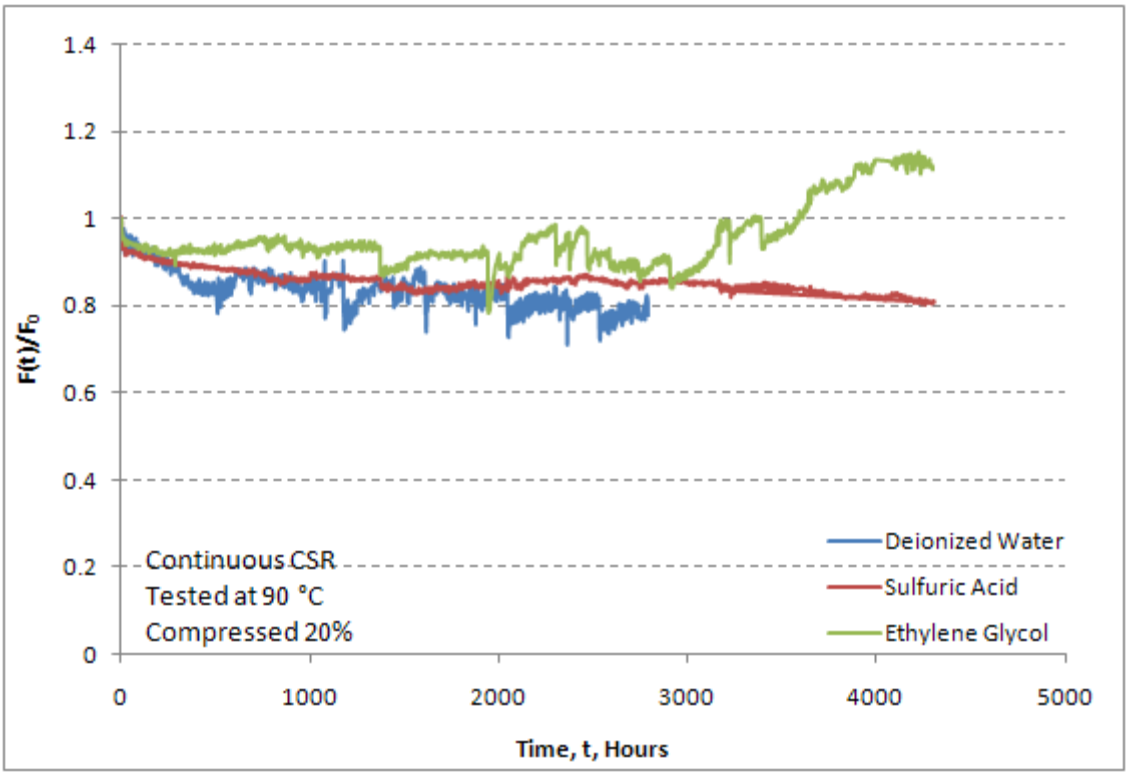

Figure 12: Stress relaxation in environment from continuous fixture

The continuous fixture has been collecting data for over 4000 hours, and allows a more accurate prediction of the initial sealing force as data is being collected throughout the loading cycle. After 2000 hours, specimens in sulfuric acid and deionized seemed to have reached a plateau of 85% and 80% of the restoring force, respectively. Samples aged in ethylene glycol shows unexpected behavior after 3000 hours. The erratic behavior seen in the continuous fixture compared to the intermittent fixture is attributed to the refilling of the container in which the fixture is held in environment; samples aged in both ethylene glycol and deionized water are much more sensitive to refilling those samples in sulfuric acid. While these fixtures are sealed

as best as possible, they are not air tight as the lower plunger is free to load the samples. This causes some evaporation of the environment and is causes a need for refilling. The containers are refilled with their respective liquid environment; however it is assumed that since these liquids show evaporation the concentration changes as the test continues. The refilled liquid is heated to 90°C, however, for the case of samples aged in ethylene glycol, the percent by volume of EG compared to water is changing as the test is run as the concentration is unknown in the fixture. This does not seem to affect the sulfuric acid environment. One possible reason for this is the ethylene glycol solution is denser than the other solutions and the density is increasing with an increase in concentration. As the density of the liquid increases, the restoring buoyancy force increases which could result in an increase in the restoring seal force. This effect was investigated by estimating the buoyancy force for samples in a 50/50 ethylene glycol/ deionized water solution and compared to samples in 100% ethylene glycol whose specific gravity is 10395 N/m^3 and 11000 N/m^3, respectively. This calculation was carried out using Equation 3 where V is the submerged volume and γ is the specific gravity of the liquid.

$$F = \gamma V$$

Equation 3: Archimedes' principle for buoyancy

The volume for this calculation consists of the SMOR'S, the washers, and the lower piston, a total volume of approximately 3.23 x 10^{-5} m^3. The difference in buoyancy force for a pure ethylene glycol mixture in comparison to a 50/50 mixture is only 0.0195 N, which is small in comparison to the initial force of 32.5 N. Another explanation for this increase could be that the EG samples are swelling over time, however, since the relaxed stack for the intermittent fixture seen in Figure 11: Stress relaxation in environment from intermittent fixture does not exhibit this behavior this explanation is unlikely. Stress relaxation on the intermittent fixture has been evaluated for samples aged in air at both 90°C and 120°C as seen in Figure 13.

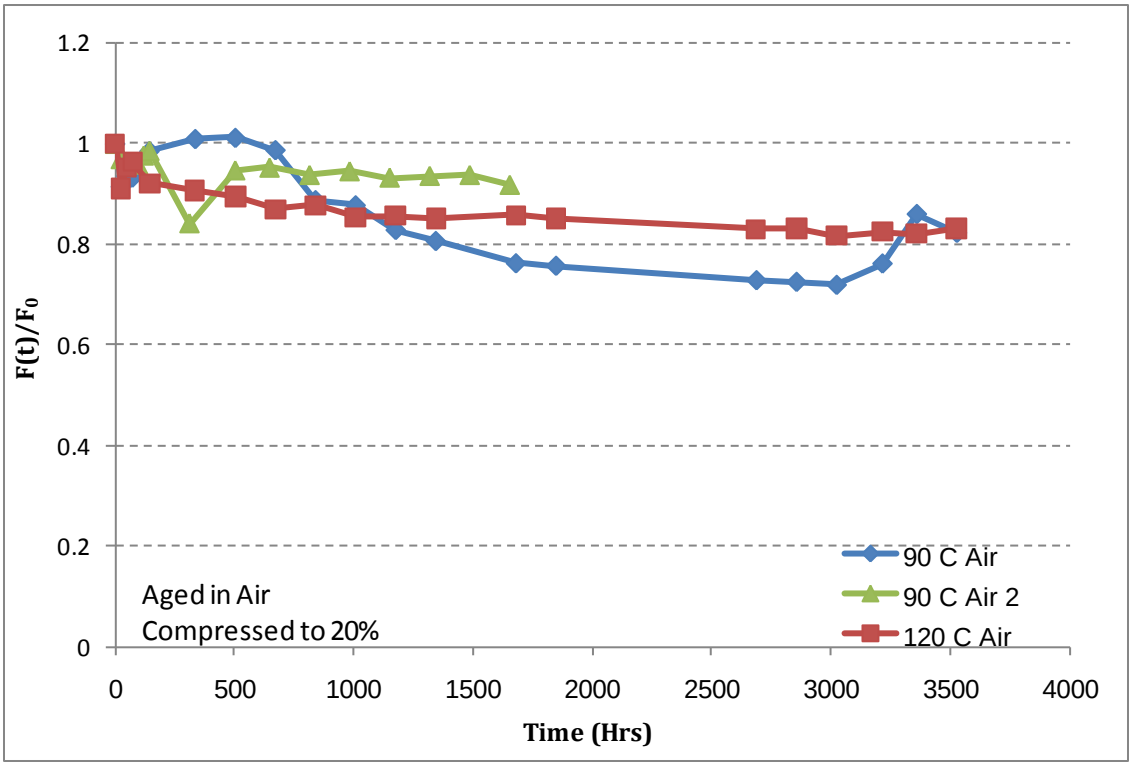

Figure 13: Stress relaxation in air from intermittent fixture

From Figure 13 it can be seen that the behavior of the stress relaxation in the intermittent fixture has erratic behavior after extended periods of time for 90°C air. For this reason, the 90°C intermittent stress relaxation fixture was restarted using an additional test frame. Currently, we can see in Figure 13 that the restarted data is showing similar trends to the stress relaxation of samples in 120°C air, however, the relaxation is taking place at a slower rate which is to be expected for lower temperatures. Additionally, the 120°C air-aged samples plateau at approximately a 17% force decay after a period of 2500 hours. For 90°C samples the plateau value is not clear as after 3000 hours, an increase in the normalized relaxation force is observed. This increase may be attributed to varying frictional effects in the 90°C stack from loading/unloading cycles.

2.4.4) Uniaxial Tension Results

Tensile strength, ultimate strain and secant modulus at 100% strain were measured and calculated for each tensile test. Comparing these mechanical properties as a function of aging time, environment and strain to those of the as-received material can provide an insight into the durability of the material. Engineering stress is calculated from Equation 4 where F is the load applied and A_0 is the initial cross-sectional area.

$$\sigma = \frac{F}{A_0}$$

Equation 4: Equation for uniaxial engineering stress

The strains for the samples were recorded directly from the laser extensometer with a resolution of 0.25 microns. Since the laser extensometer has a limited range of extension, and the samples undergo large deformations, the strain obtained from the laser was correlated to the crosshead displacement. This was performed by plotting the strain from the crosshead vs. the laser strain and correcting such that the slope of the line is equal to one as seen in Figure 14.

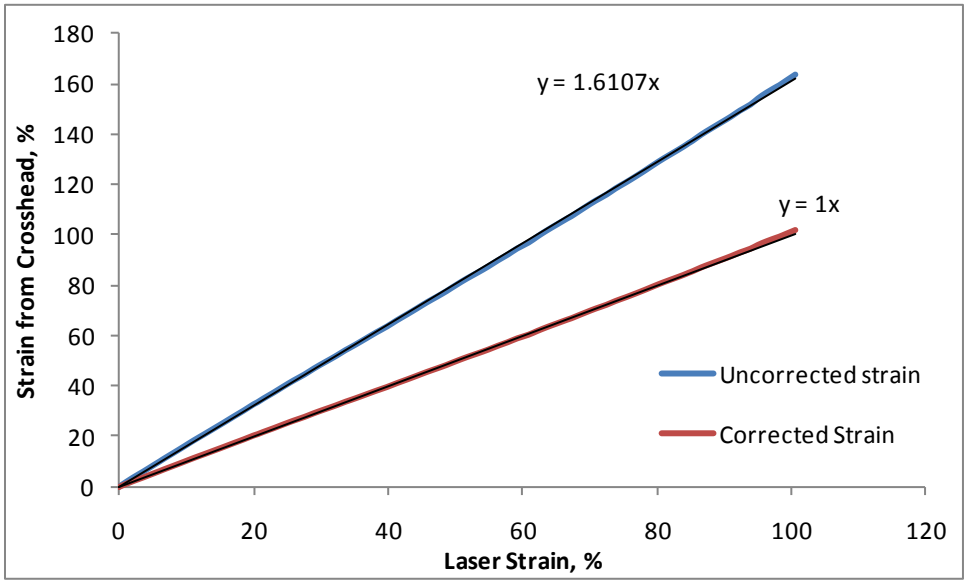

Figure 14: Correction of strain from laser extensometer to crosshead displacement

Each property is plotted versus time for each prescribed strain and is compared to the as-received samples. An example of this for samples aged in sulfuric acid can be seen in Figure 15, where tensile strength is plotted versus aging time. Note that for all plots shown the error bars represent ± one standard deviation.

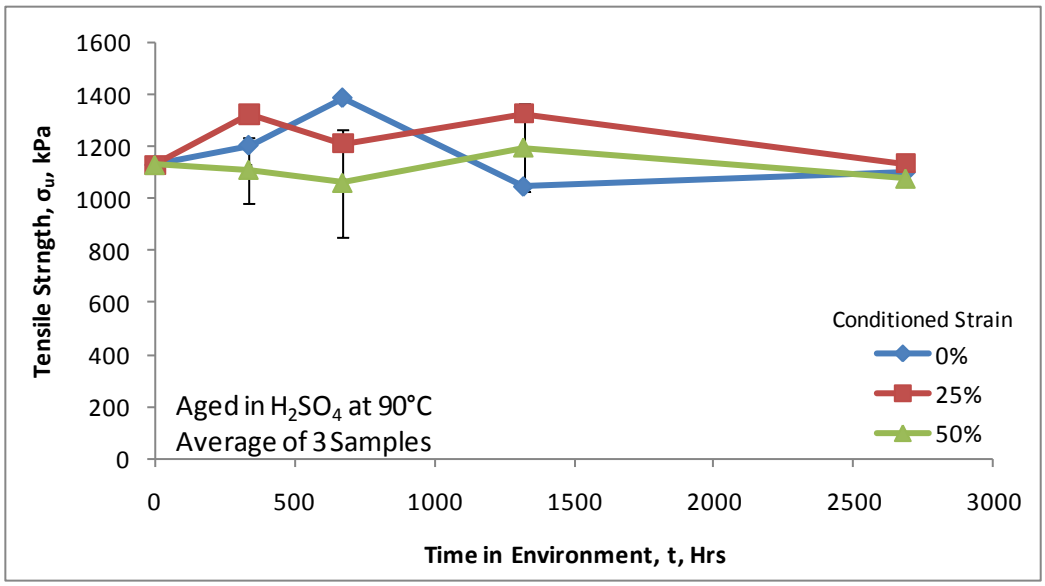

Figure 15: Tensile strength for sulfuric acid samples versus aging time

However, it is hard to draw conclusions from each separate environment versus time plot as the results across the samples vary. When looking at the ultimate aging time for each property a comparison can be made. The ultimate strength at failure is plotted for each prescribed strain and environment at the maximum aging time of 2700 hours in Figure 16.

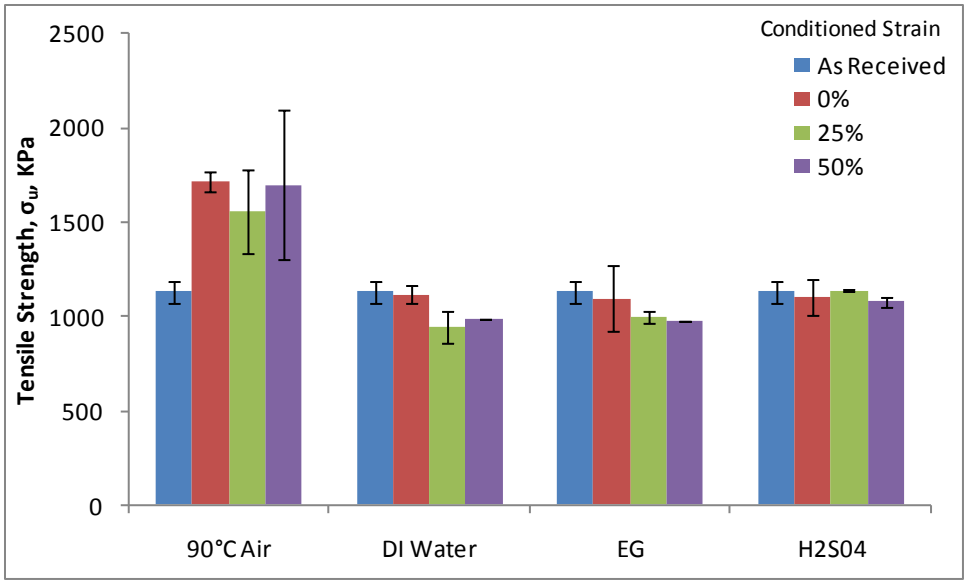

Figure 16: Comparison of tensile strength versus environment

It can be seen that for all liquid environments and prescribed strains, the tensile strength after 2700 hours shows a small decrease. Generally, samples aged in liquid with a prescribed strain show more of a decrease in ultimate strength compared to samples aged free of strain. These samples can undergo chain scissioning and crosslinking, which could the ultimate strength values. Also, a small decrease in tensile strength when compared to the as-received material is observed, which suggests that the ultimate strength of liquid-aged samples is not affected by these aging conditions. The tensile strength evaluated at the longest aging time for samples aged in 90°C air shows an increase in the ultimate strength which is contrary to the results seen for samples aged in liquid environments. This is suggestive of an increase in crosslink density for samples aged in air compared to those aged in liquid and was observed earlier from the momentary stiffness results. Figure 17 compares the ultimate strain, to different strain and environments.

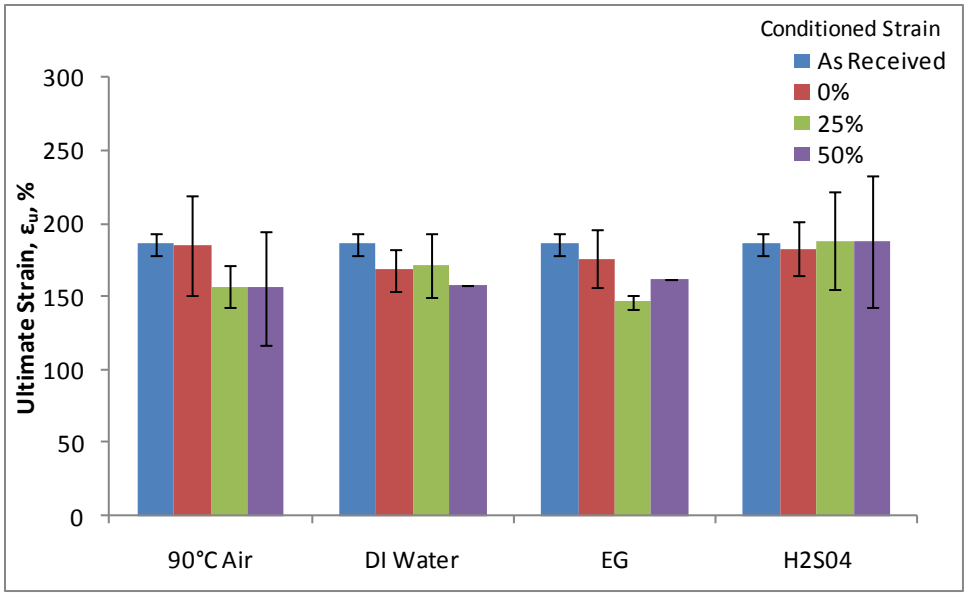

Figure 17: Comparison of ultimate strain versus environment

The ultimate strain and tensile strength plots show a similar trend except for air-aged samples. The drop in ultimate strain combined with an increase in ultimate stress for air-aged samples suggests a dramatic increase in the material's modulus, which is clearly seen in Figure 18.

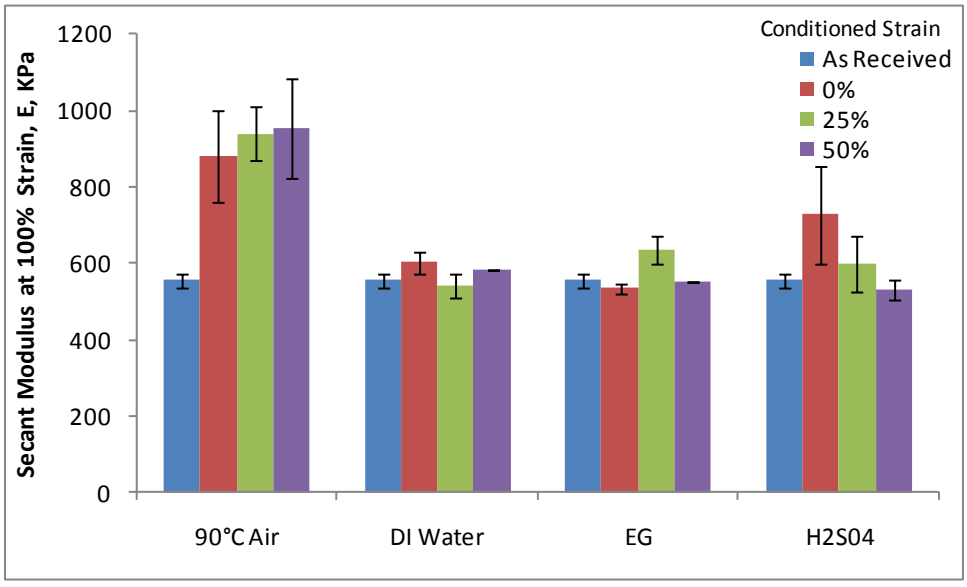

Figure 18: Comparison of secant modulus at 100% strain versus environment

These results can be explained by chain scissioning and re-crosslinking. Similar to the intermittent stress relaxation, the polymer chains in the strained sample may break and reform

and could create a secondary network. Removing the strain in these samples and then testing evaluates the sum of both the remaining original network and the newly formed network. For this case, an increase the materials' behavior in response to loading is indicative of a secondary network being present as the new network can now carry a portion of the load. Additionally, physical aging can be accompanied by increases in stiffness, yield stress, density and viscosity [16-17]. This can be seen for all aging conditions as the secant modulus shows an increase or similar value when compared to the virgin material. A dramatic increase in the secant modulus at 100% for the air-aged samples is observed and follows the results from the momentary stiffness results performed above.

2.5 Conclusion

Viscoelastic properties have been evaluated for a hydrocarbon elastomeric molded seal using momentary and relaxed stress response from two different test fixtures. The constitutive properties of these materials have also been compared over varying aging times, strain rates, and environments. For the stress relaxation tests, by comparing the momentary and relaxed states, a comparison can be made between rate of additional crosslinking in the presence of chain scissioning and chain scissioning effects alone. From relaxation tests, it was determined that for momentary stress relaxation, the samples in liquid environment showed little change in restoring force suggesting that the rate of chain scissioning is equivalent to that of additional crosslinking or non-existent. For momentary stress relaxation for air-aged samples, it was seen that the rate of crosslinking was higher than that of chain scissioning as the momentary modulus was increasing. Stress relaxation tests, in liquid environment showed 16% decay in load over time. Additionally, these samples illustrate small changes in relaxation after an extended period of time suggesting, that the chemical degradation process has slowed after 2700 hours. Stress relaxation tests in air showed a similar dependence on temperature, compared to the momentary tests where the rate of degradation was higher for 120 °C samples compared to 90

°C. From the uniaxial tension tests, small decreases in the ultimate properties of the material occur after 2700 hours in strain and aged conditions. However, due to additional crosslinking in the strained states, the secant modulus at 100% strain of the material experiences an increase for all cases.

Chapter 3: Effects of Aging on Tearing Energy

3.1 Introduction

An important aspect when evaluating a material's mechanical properties is tearing energy. Tearing energy of elastomers can be evaluated using a variety of test methods, but for this case the trouser tear test was utilized to determine the tearing energy and how aging affects the fracture properties. The tearing energy was evaluated for a range of crack growth rates and temperatures in order to determine the master curve of the fracture energy. By comparing the fracture energy master curve for the as-received material to a material which has been aged, insights into the durability of a material can be gained, specifically about the resistance to subcritical cracking. Additionally, testing in a liquid environment can affect a material's response to crack growth so samples have also been tested in their aged environment to examine this effect. An understanding of the effects of crack growth rate, testing temperature and both aging and experimental environment can be used to predict crack growth under a variety of conditions.

3.2 Background

The mechanical performance of elastomers is not only affected by constitutive response but can also be affected by tearing energy. Tearing energy, which is a measure of a material's resistance to tear propagation, has been used to characterize the resilience of the elastomer to crack propagation [18]. In synthetic and natural materials, the stress is distributed unevenly and fracture takes place along the weakest part, where the strength of a sample is determined by the most critical defects[12]. The differences between predicted and actual strengths develop due to these defects which can cause local stress peaks. These flaws are generally physical discontinuities that include cracks or local material defects as well as discontinuities in the elastic modulus. Fracture occurs when flaws become capable of propagating [19]. Crack

growth occurs when the stress at the tip of the fracture point reaches a critical value[20]. For brittle materials, Griffith's theory states that a crack in a strained sample will grow if the strain energy released by a small increment of crack growth is greater than the amount of surface free energy [20-22]. This theory implies that the surface is formed with no dissipation of energy into other forms other than surface energy which is not applicable for rubber like materials.[20] For these types of materials, no plastic deformation occurs near the tip of the crack, its growth involves a dissipation of energy which is several orders of magnitude greater than the surface energy which implies that Griffith's theory must be extended for rubber-like materials[23].

Generally, the tearing energy can be affected by many different processes. The degree of crosslinking can affect the tearing energy [24]. At high aging times and temperatures, the degree of crosslinking could increase, which could cause a restriction in chain motions. If this occurs, the network then becomes less capable of dissipating energy, and the elastomer fails in a more brittle manner with low elongation and tearing energy [25]. Tearing of elastomers involves two processes, the initiation of small flaws and the growth of these flaws due to an instability at the crack tip [26]. For viscoelastic materials, crack growth is controlled by temperature, rate of tearing, and crosslink density and can be slowed by energy dissipation, strain-induced crystallization or deviation of the tear tip [26]. Additionally, environment can play a role where chemical interactions can change the composition and physical properties of a material as chemical bonds can break and reform/rearrange, affecting the tearing strength [12]. Stick-slip fracture is a commonly observed phenomenon in fracture tests and can affect fracture results. It is characterized by erratic crack tip velocities (cycles of fast, unstable crack propagation and arrest) resulting in crack growth jumps. Stick-slip crack propagation is characterized by an increase of load with no crack growth followed by a sudden decrease in load as the crack propagates unstably and then arrests [27]. A knotty tear, observed in many different works, can also effect tear propagation of elastomers. A knotty tear occurs due to a

material's preference towards strain-induced crystallization during loading and could cause variation in the fracture energy [28-29]. To counter these effect fracture tests are typically performed using specimen configurations whose compliance is linear in the crack length such that the crack growth stability condition is automatically satisfied [30]. Additionally, tearing strength of elastomers has been shown to reach a lower limit, termed a threshold value where dissipative processes are minimized. Threshold values can be determined at low rates of tearing, high temperatures and when the material is highly swollen with a low-viscosity liquid. It is generally assumed that the polymer network strands governing small-strain elastic behavior are responsible for tearing strength under threshold conditions [31]. Since tearing energy can be critical to durability, it will be evaluated to determine resistance to crack propagation.

3.3 Experiment

To characterize tearing energy, trouser tear tests were performed at a variety of temperatures and rates and to determine the complete characterization of the tearing energy of this system. Tearing energy was examined for the as-received materials and compared to samples that have been aged in environments at elevated temperatures. Furthermore, tests have been conducted in the materials aged environment for samples aged in deionized water. Additionally, to examine the low tearing energies, tear tests have been performed in a tank to obtain low tearing energies which correlate with slow crack growth.

3.3.1) Materials:

The material tested was a hydrocarbon elastomer provided by Henkel Corporation (Rocky Hill, CT). The material is a heat cure system which is heated to 120°C for two to three minutes for sufficient crosslinking to occur for mold removal and is then post-cured at 130°C for one hour. For trouser tests, the material was prepared in 200mmx200mmx2mm slabs with 10 mm reinforcing fiber strips which are non-woven polyester fabric (Freudenberg- NonWovens PN# FS2227, Plymouth, MI) that has been embedded at the midline of the sheet as seen in

Figure 19. The elastomeric material has been reinforced in the legs to prevent the crack from propagating outside of the sample also since the fabric is less compliant then the elastomeric material we can assume that the legs are inextensible in comparison to the tearing region. Reinforcing the legs of a rubber tear specimen has been performed by Loha as improves the reproducibility and reduces the variation of the results [32]. Additionally, reinforcing trouser samples has been used to control stick-slip and crack path deviation [29].

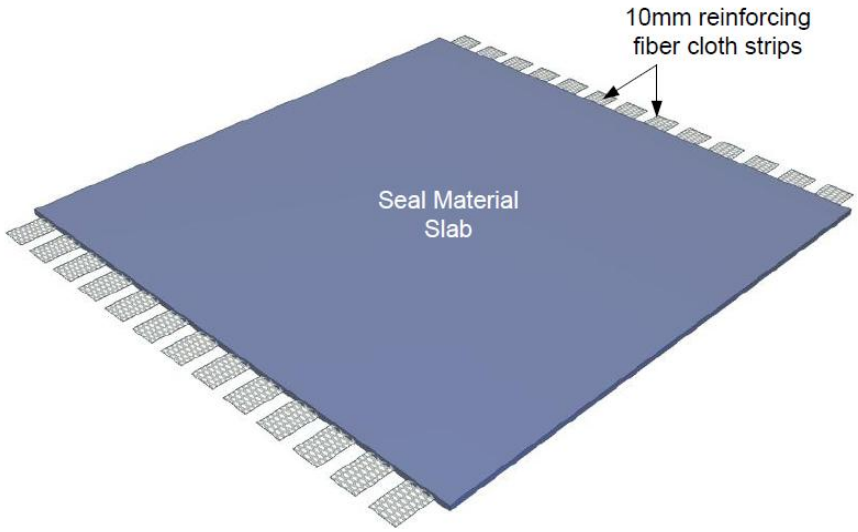

Figure 19: Reinforced hydrocarbon slab for trouser experiment [13]

3.3.2) Sample Preparation:

Specifically, for this experiment, trouser tear samples were used to test fracture energy. Trouser samples were prepared by cutting a 200mmx25mmx2mm specimen seen in Figure 20 from the reinforced slab seen in Figure 19.

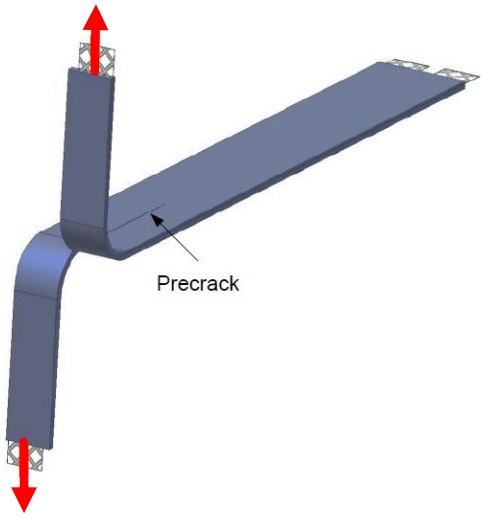

Figure 20: Example of trouser sample [13]

These samples are free of reinforcement in the center region such that the crack can propagate in this area. A notch for the beginning of the crack tip was cut using a razor blade at one end of the sample.

3.3.3) Test Procedure:

Trouser tests were conducted following ASTM standard D624. The legs of the sample were gripped using binder clips, and the samples tested in air were tested using an Instron 4505 with a 100 N load cell and a temperature controlled Thermotron oven. Samples tested in deionized water were tested on an Instron MicroTester 5848 with a 50 N load cell as seen in Figure 21. The MicroTester was configured horizontally to perform testing in a liquid. The liquid environment is contained in a stainless steel container which is heated through the use of a hot plate (Corning, Corning, NY). The temperature of the liquid environment is controlled using a custom made temperature feedback controller.

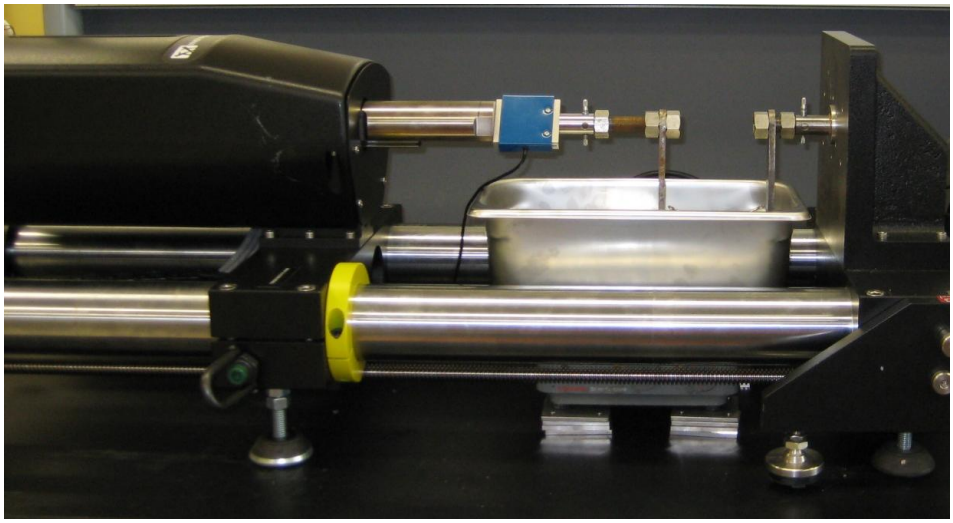

Figure 21: Experimental setup for trouser tests in environment

Tests were conducted on as-received material and on specimens that had been aged for 10 weeks in 90°C air, 120°C air, 90°C deionized (DI) water, 90°C 50/50 ethylene glycol, and 90°C 0.1 M sulfuric acid. Samples were tested at several rates from 1 mm/min to 1000 mm/min as well as several temperatures. A loading displacement plot obtained from a trouser test performed in air at room temperature conducted at rates from 1 mm/min to 1000 mm/min can be seen in Figure 22.

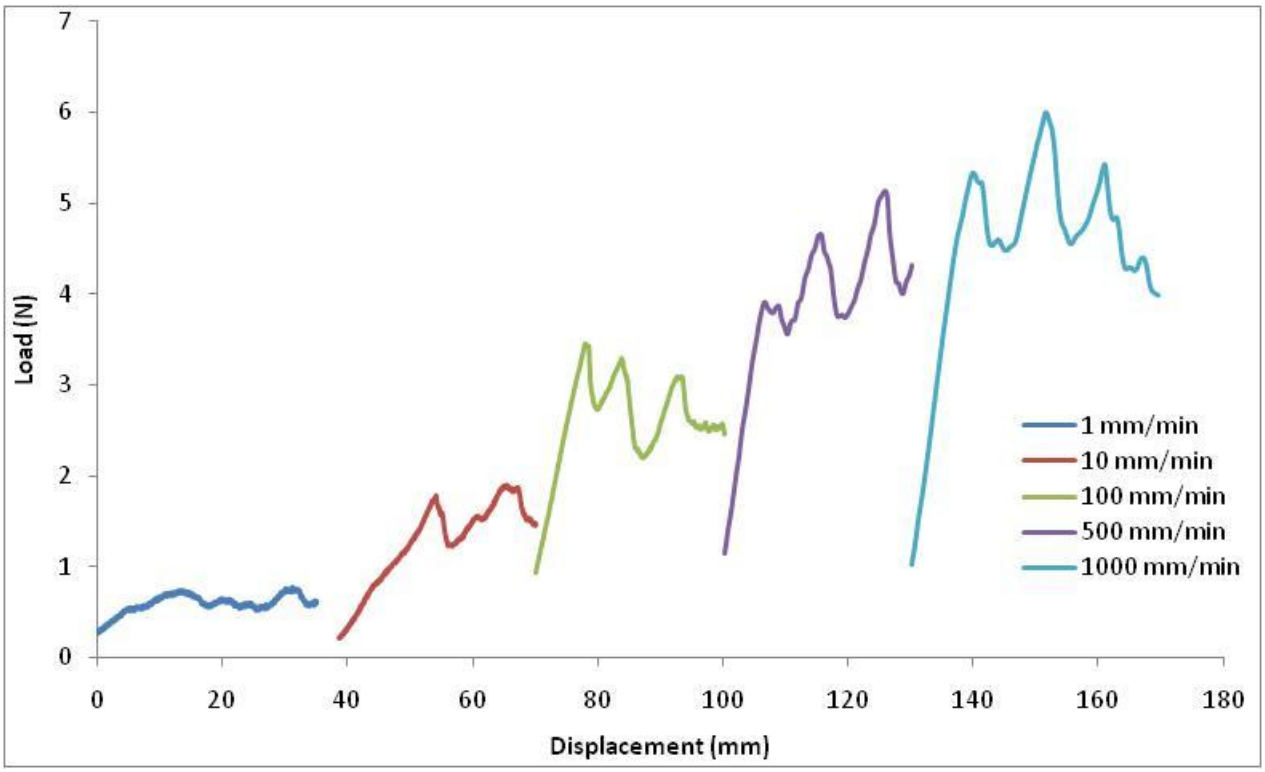

Figure 22: Load displacement plot from trouser tear test conducted in air

For the as-received material, the samples were tested from -30°C to 120°C. For those samples that had been aged, the materials were tested in a reduced temperature range from 23°C to 95°C. The testing matrix was reduced because the area of interest for tearing energy was observed in this temperature range. In order to determine a threshold value, a custom-built fixture was designed, as seen in Figure 23, to allow trouser tear tests to be run in a liquid environment at very slow rates. The tank used is a 27cm x 26.5cm x 7 cm thin layer chromatography tank (Sigma-Aldrich, Milwaukee, WI) which has been filled with deionized water and allow to equilibrate to 90°C by placing the entire fixture in a convection oven (Precision Thelco, Englewood, CO). One end of the samples was gripped using binder clips suspended above the tank and the other ends were loaded using bolts of varying weights. The samples are allowed to equilibrate at temperature for one hour before loading. The crack growth rate was measured using a digital camera from pictures taken of the specimen every 15 minutes. The

crack growth rate is recorded over an extended period of time and is averaged across each specimen.

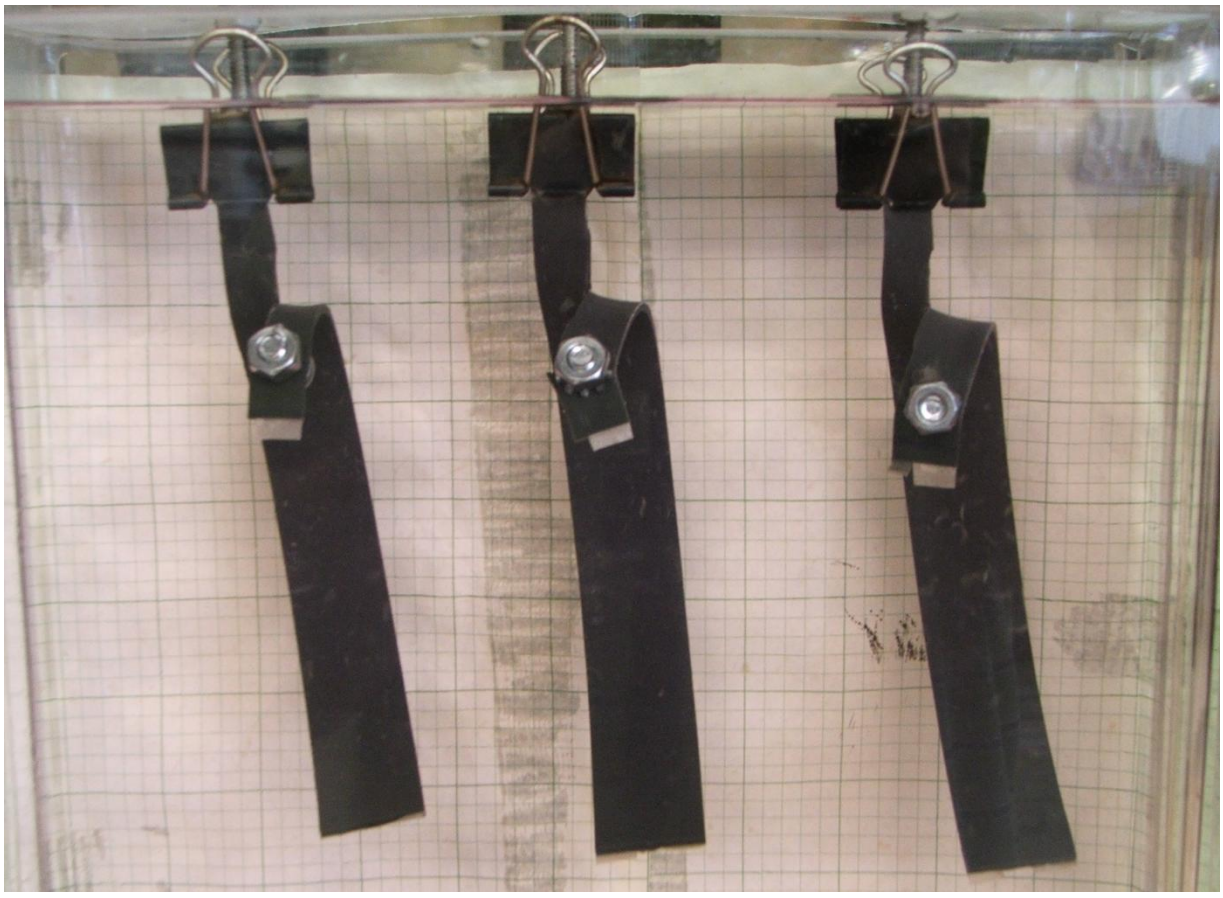

Figure 23: Custom built fixture for trouser tests at slow rates

Additionally, dynamic mechanical analysis (DMA) tests have been run to compare the shift factors of the as-received material to the shift factors obtained from fracture tests. Samples were tested using a DMA 2980 and in a shear sandwich configuration. The DMA test was run using a temperature step and frequency sweep. The temperature ranged from -50°C to 130° and was stepped by 10°C with a 5 minute equilibration time at each temperature. The frequency was swept from 0.1 Hz to 85 Hz with two steps per decade.

3.4 Results and Discussion

For each fracture test, the tearing energy, also known as the strain energy release rate, was plotted versus the crack growth rate on log-log axes. The tearing energy, $\mathcal{G}$, is considered to be the rate the stored elastic energy decreases in the fractured material and is defined in Equation 5 where U is the stored elastic energy and A is the area of one crack face.

$$\mathcal{G} = -\frac{\partial \mathrm{U}}{\partial \mathrm{A}}$$

Equation 5: Strain energy release rate

For this test, an average of the load once the crack begins to propagate is used to determine the strain energy release rate. The start of crack propagation is taken to be the first maximum in the loading curve below which tearing does not occur. The average crack load is the average of the force from the start of crack propagation to the end of the test ran at a given rate. For these samples, Equation 6 was used to calculate the fracture energy, where λ is the stretch in the legs equal to the current length over the initial length, P is the force on the specimen, u_0 is the strain energy density in the legs, A_0 is the cross-sectional area of one leg, and h is the sample thickness.

$$\mathcal{G} = \frac{2\lambda P - u_0 A_0}{h}$$

Equation 6: Strain energy release rate equation for trouser samples

For reinforced trouser specimens where the legs have been reinforced with fiber, the legs can be assumed to be inextensible in comparison to the tearing region. This condition is such that for the strain energy release rate equation, the stretch in the legs, λ, is equal to 1 and the strain energy density in the legs, u_0, is 0. This allows us to simplify Equation 6 to Equation 7.

$$\mathcal{G} = \frac{2P}{h}$$

Equation 7: Simplified strain energy equation for reinforced trouser samples

The force on the specimens for this procedure is an average across a single sample from when the crack begins to propagate at a specific rate to when the crack is stopped. This force is also averaged typically over three samples. Results show some variation once the crack has begun to propagate, this unstable crack propagation is characteristic of a knotty tear as the decreases in loading is not as pronounced as seen for stick-slip phenomenon. However, a knotty tear is characteristic of strain induced crystallization which is not seen in the uniaxial tension tests performed in Chapter 2. Another possible explanation for the unsteady crack growth could be that the elastomer tested is a composite polymer which includes fillers and particulates. The addition of these particles could also have an effect on the unsteady crack propagation. The crack growth rate, $\frac{\partial a}{\partial t}$, for samples where the legs are inextensible is considered to be half of the testing machine's crosshead speed. The fracture energy as a function of crack growth rate has been plotted in Figure 24 for the as-received material.

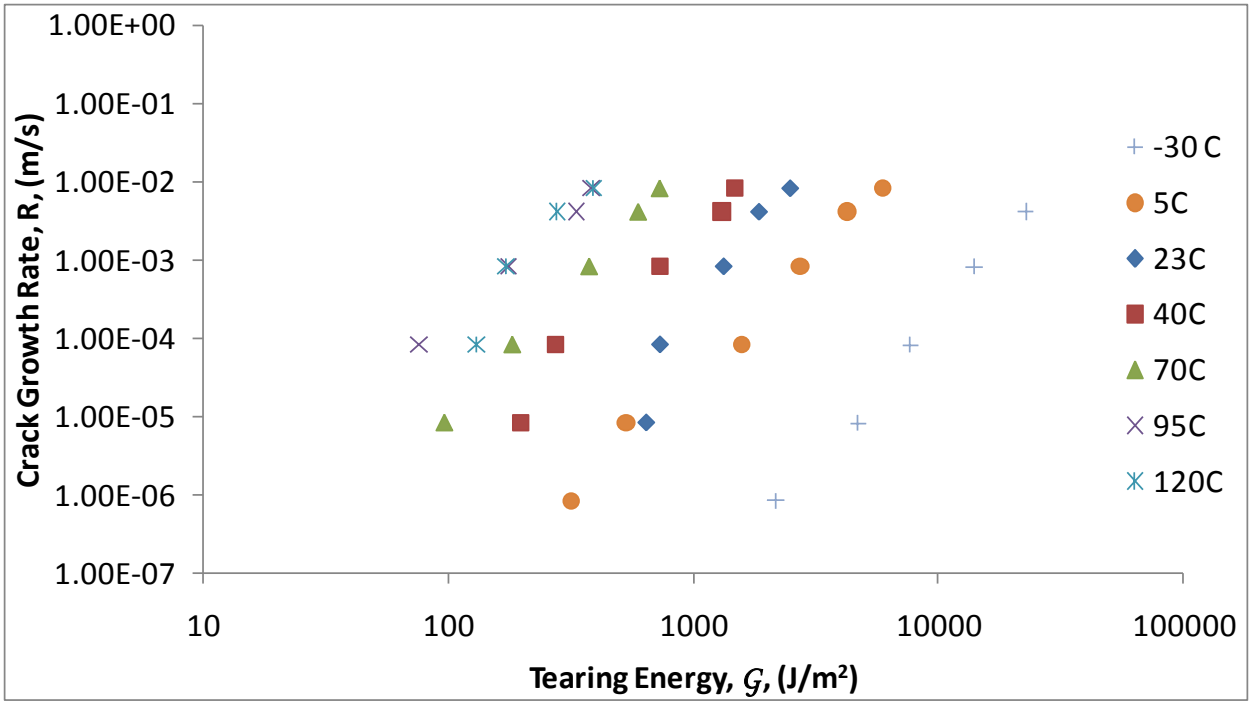

Figure 24: Plot of fracture energy as a function of crack growth rate

Since these materials are viscoelastic in nature, it can be seen from Figure 24 that the material is both temperature and time dependent. To create a master curve of this data, time-temperature superposition was performed on the fracture data by manually shifting the fracture results from a reference temperature and then fitting these shifts using the WLF equation seen in Equation 8: WLF Equation.

$$Log\ \ a_T = \frac{-C_1(T - T_{ref})}{C_2 + T - T_{ref}}$$

Equation 8: WLF Equation

A WLF shift on the fracture data using a reference temperature of 95°C, as seen in Figure 25, yielded values for C_1 and C_2 of 6.5 and 241°C, respectively. Where the error bars shown are representative of the variation coefficient for each temperature tested.

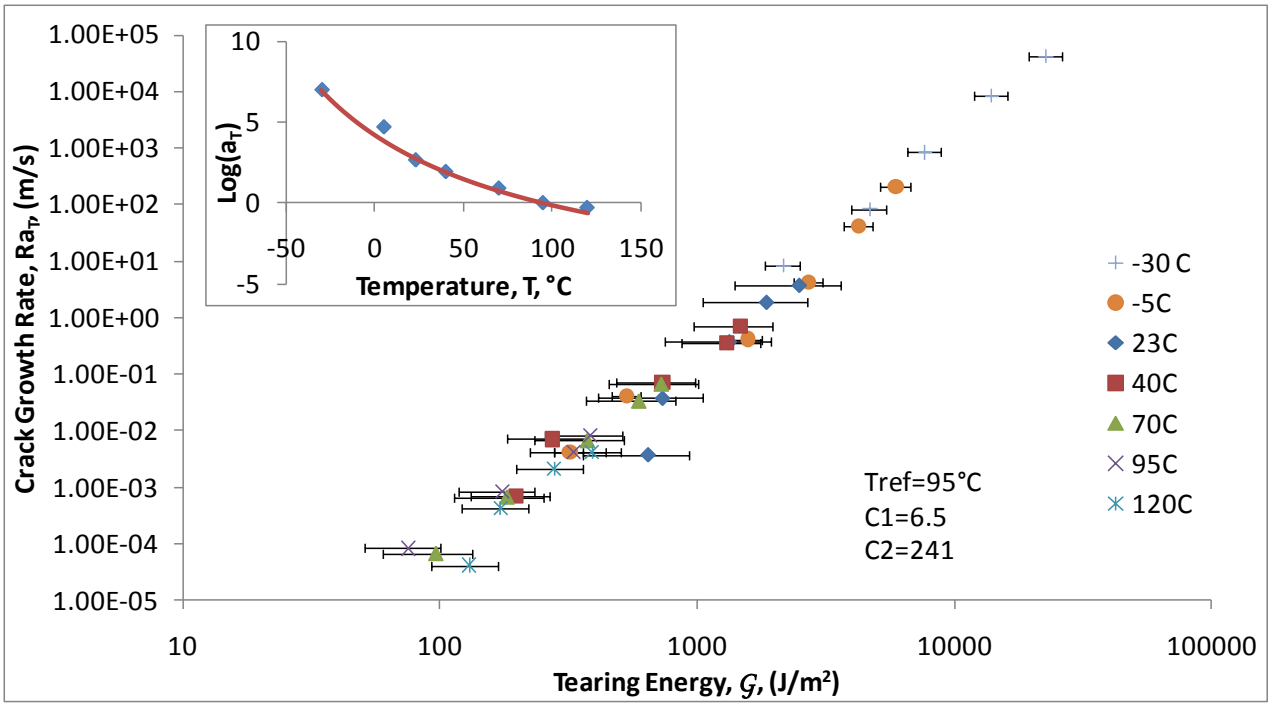

Figure 25: Master curve of the as-received material tested in air

By shifting the universal constants to the reference temperature we find that the C_1 and C_2 values from the universal constants are 9.9 and 211°C respectively which compare well to 6.5 and 241°C which were obtained from the as-received tearing energy shift factors. The master curve of the fracture energy shows a very linear response to crack growth rate.

In order to examine the fracture surface, scanning electron microscopy images of trouser tear samples have been captured seen in Figure 26.

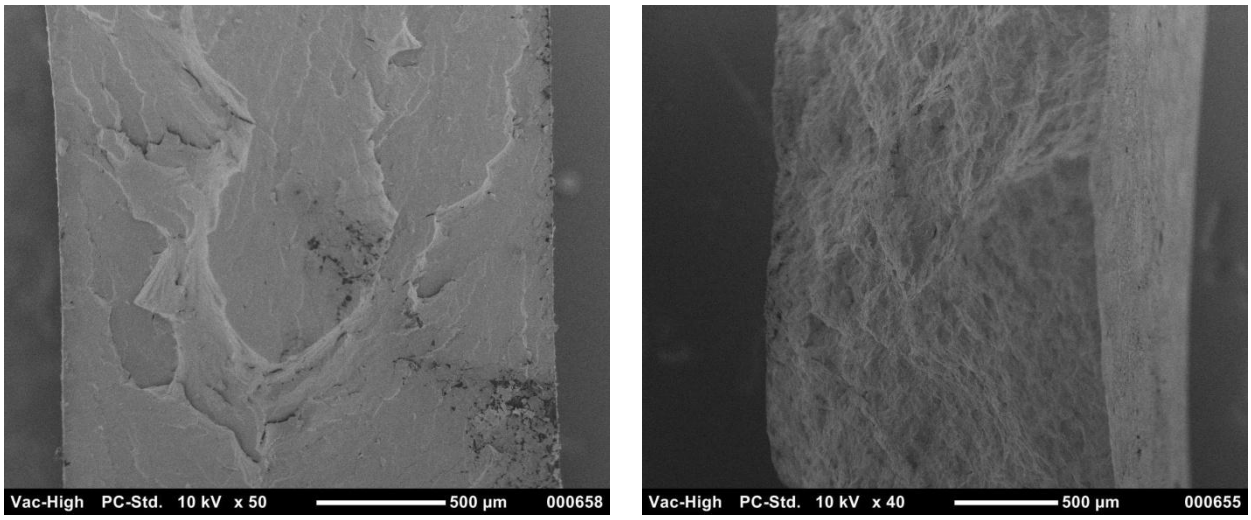

Sample tested at 23°C Sample tested at 90°C

Figure 26: SEM pictures of the trouser tear fracture surface for the as-material

As seen in the sample tested at 23°C, small voids are present in the material; these voids could be responsible for some of the variation seen in the fracture energy results. If the sample is not continuous, the fracture energy and crack growth rate in these regions would be different in comparison to those with material. Specifically, if these voids are present along the crack surface, the force required to tear the specimen would exhibit variation similar to what is seen in Figure 22.

As the tearing energy becomes closer to the lower limit of the test, i.e. high temperatures and slow crack growth rates, the beginning of a threshold can be expected; however, from the data set presented in Figure 25, it is unclear if a threshold is present. In order to examine this more closely, tearing tests after environmental aging as well as in environment have been conducted to examine this phenomenon more closely. A comparison of the master curves of the as-received material to the aged material can be seen in Figure 27.

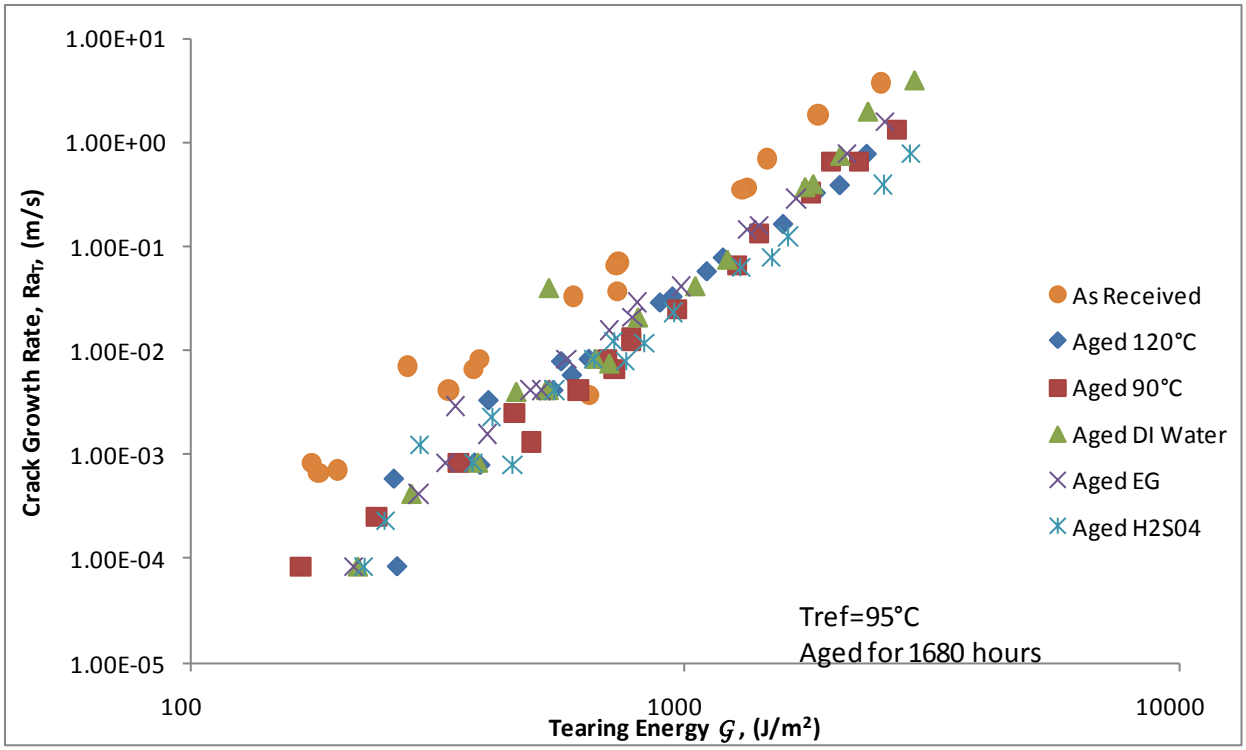

Figure 27: Comparison of master curves of fracture energy for as-received material to aged material

It can be seen that as the samples are aged, the tearing energy of these polymers increases. This could be a function of increased crosslink density or sample conditioning. Furthermore, if the crosslink density increases without restricting the elastomer's ability to dissipate energy, the tearing strength of these materials could increase. Additionally, as seen in Figure 27, the onset of a threshold value is still unclear, for this reason testing has been conducted in deionized water and the master curve for the fracture energy can be seen in Figure 28.

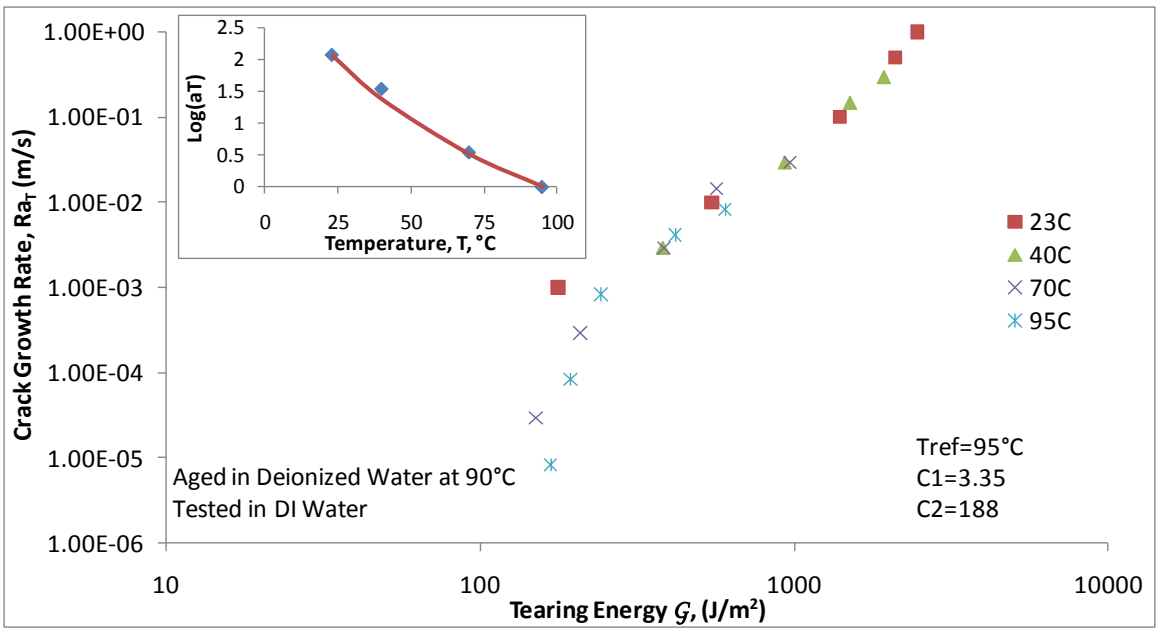

Figure 28: Master curve for samples aged in deionized water and tested in deionized water

From Figure 28, a threshold value can begin to be seen at around 170 J/m^2. Incorporating the trouser results from testing in the tank as seen in Figure 29 the threshold value appears to be lower at approximately 80 J/m^2.

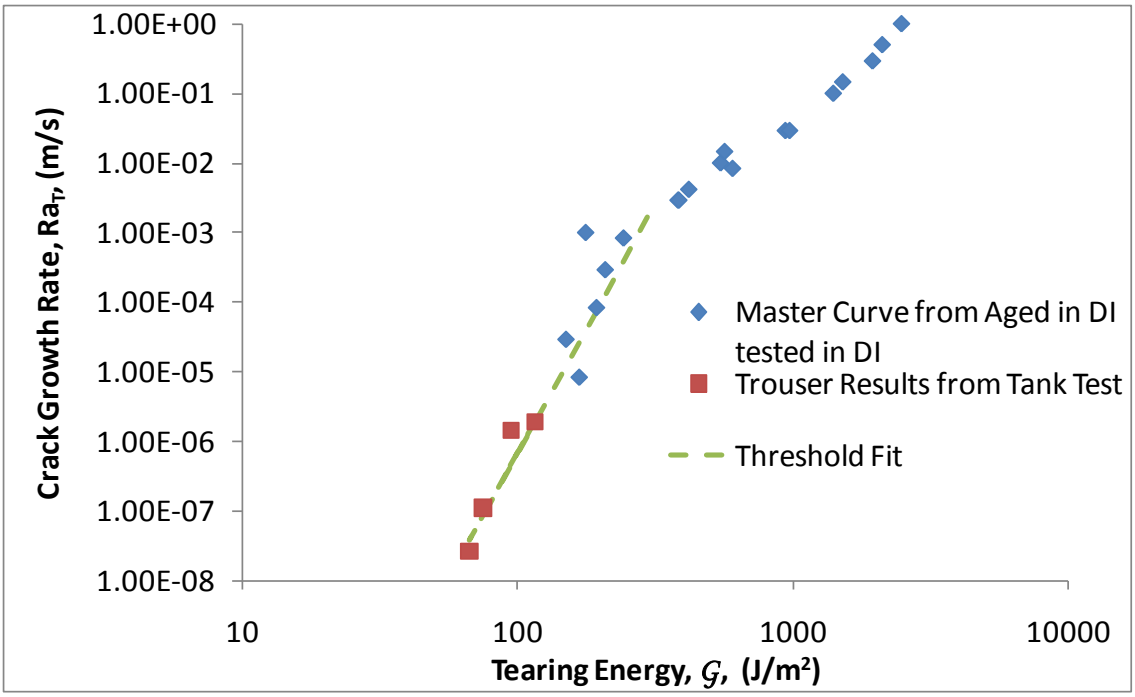

Figure 29: Comparison of master curve for samples tested in tank and those tested in deionized water using the MicroTester

The reasons that this threshold value is only seen when tested in liquid environment are complex. Tests conducted in environment are carried out using an Instron MicroTester 5848 which has a higher precision displacement control compared to the Instron 4505, which was used for trouser tests conducted in air. The MicroTester has a precision displacement control of 20 nm which is 100 times more precise than the Instron 4505, which has a displacement control of 0.02 mm. Additionally, the load cell used for the tests carried out in environment has half of the capacity of the load cell used for those tested in air. This causes the resolution of the fracture load to be more accurate for tests carried out in liquid in comparison to air. Furthermore, testing in liquid environment could have an effect on the tearing energy as it could change the surface energy, which from Griffith's theory could affect the elastic energy necessary for crack growth. Finally, since these threshold values occur at such a low tearing energy, the loads required to achieve threshold are so small (approximately 0.15 N) that the weight of the sample may come into effect. It was assumed that the force exerted by the grips to produce tearing was greater than the affect of the weight of the specimens. However, at such low tearing energies and because the threshold is only observed when testing in liquid environments where buoyancy and, for the case of the MicroTester, horizontal loading the weight of the elastomer could be affecting the appearance of the tearing threshold.

Since these materials are expected to behave in a viscoelastic manner, the shift factors should compare regardless of the individual test performed on the material. Dynamic mechanical analysis was performed on three sample sets and results for the storage modulus can be seen in Figure 30.

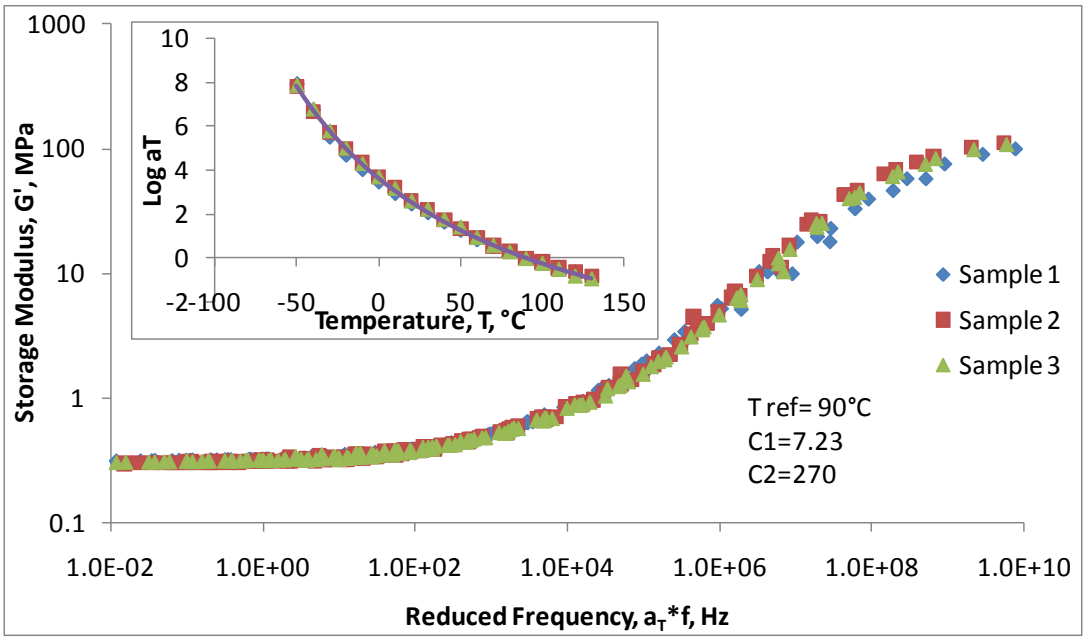

Figure 30: Storage modulus results from Dynamic Mechanical Analysis of as-received material

A comparison of the shift factors from the as-received fracture energy to dynamic mechanical analysis can be seen in Figure 31.

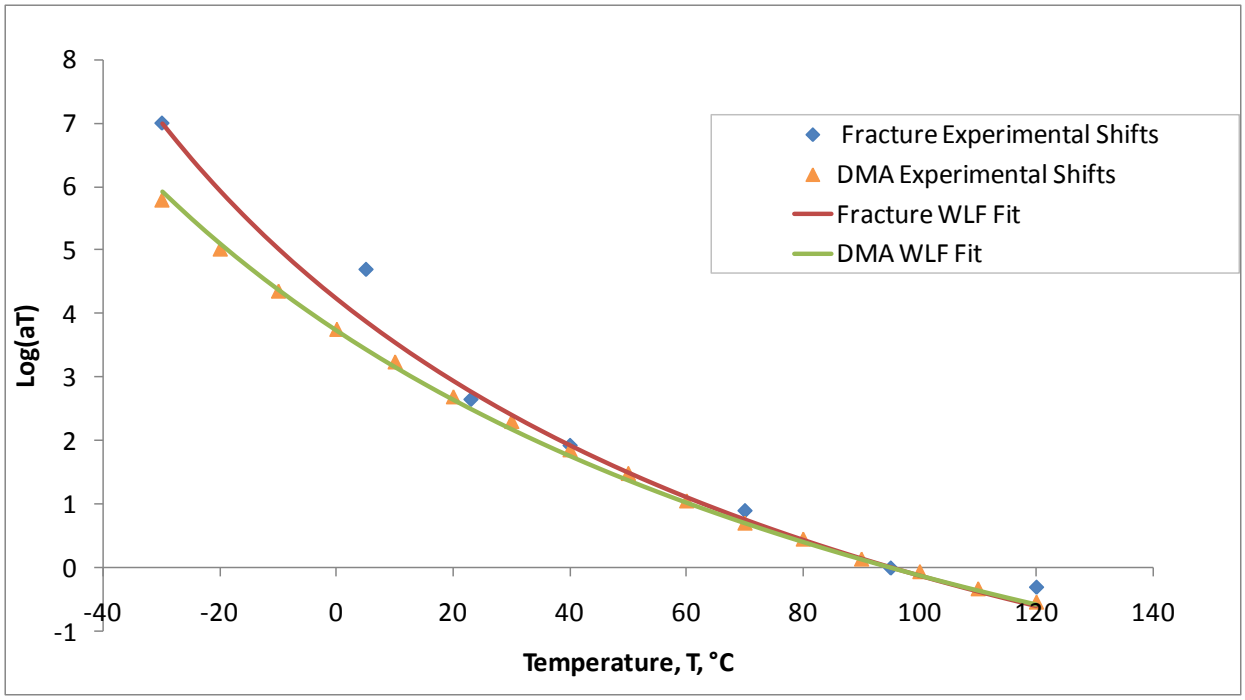

Figure 31: Comparison of shift factors from fracture energy to DMA

As seen in Figure 31, the DMA shift factors agree well with the shifts from the as-received material tested in fracture. The fact that the shift factors from DMA compare well to the fracture energy shift factors shows that even though both the fracture energy and the material response to a dynamic load are governed by different phenomenon, the viscoelastic effects, specifically the effect of free volume, which governs this materials, not only affect both the constitutive and fracture response in a similar manner but affects them both almost equally.

3.5 Conclusions

Fracture properties of a hydrocarbon based elastomer have been evaluated using trouser tests. Trouser tests were performed under several rates and temperatures to determine the tearing strength as a function of aging. Testing was also carried out after aging in various environments to determine the materials durability to tearing. Furthermore, it was observed that this behavior was shown to follow time temperature superposition and was in good agreement

with the constitutive data obtained from dynamic mechanical analysis. Results showed that for all aging conditions, the tearing energy of this material has increased for all aging environments. Additionally, fracture tests in environment shows the onset of a threshold value, below which fracture will not occur.

Chapter 4: The Effects of Confinement on Elastomers using Finite Element Analysis

4.1 Introduction

Demand for stronger and more durable sealants has increased each year as the evolution of modern architecture requires a higher demand for such sealants. Today, current architecture requires complex geometries to be structurally sealed. Elastomeric materials are commonly used for these adhesive joints as they can provide the necessary strength and bonding characteristics for an assortment of applications [33]. While these materials are used across a variety of bonded applications, a thorough understanding of the joint characteristics and material behavior must be completed before implementing a joint in a specific design. The Dreaming project in Fredrick, Maryland is an example of the implementation of complex bond geometry before a thorough understanding of the joint design. This lack of understanding caused the bonded glass sculpture to fail as shortly after installation as the joint adherend began to crack and debond from the bonded silicone rubber support layer. Cracking was present in the outer adherend especially in areas which contained large changes in sealant thickness. Additionally, delamination was occurring in transition areas from thin to thick sealant. Failure of this art project has been attributed to the large coefficient of thermal expansion of the sealant coupled with large thickness variations in the elastomer [34]. In order to examine of the effects of confinement and variable layer thickness on this elastomeric joint, finite element analysis has been performed on a relevant variety of bonded geometries. Additionally, the finite element model was extended to examine design changes which could reduce the effect of the thermal expansion of a variable thickness elastomeric adhesive while retaining the artistic geometry.

4.2 Background

Generally, the strength of an adhesively bonded joint is a function of the mode of loading and the dimensions and elastic properties of the bonded components as well as the intrinsic

strength of the interface [35-36]. Additionally, the durability of an adhesive joint requires that the joint must retain structural integrity no matter what environmental or failure mechanisms may be present [37]. For an elastomeric joint which is bonded between rigid platens and compressed or extended, the pressure loading distribution is far from uniform and is a function of the entire plate deformation field [38]. Additionally, rubber can respond differently to low and high contact pressures. Under low contact pressures rubbers can form a soft sticky surface layer, where as for high contact pressure tearing can occur, presumably due to large frictional forces [39]. Peel stresses can also become an issue when two adherends with a curvature mismatch are bonded together with an adhesive layer [40].

Furthermore, compressive stresses are generally not uniformly distributed over the surface of a compressed elastomeric material but reach a maximum in the central region due to frictional restraint which decreases towards the edge of the material [39]. When a bonded elastomeric block is compressed, the total force exerted can be thought of as the superposition of the force required to deform a perfectly lubricated block and the force generated when the surfaces of the freely expanded block are forced back to their actual bond location [41]. When deformation of a bonded elastomer occurs, it can be assumed to occur in two stages: pure homogeneous compression and shear deformation which restores the points in the plane of the bonding surface to their original position [42]. Furthermore, when a block of highly elastic material is subjected to triaxial tensile stresses exceeding a critical level, cavitations or large voids in a material can occur [43].

Since a combination of all of these effects can become complicated, mechanical design with elastomers is often performed using finite element codes as they are able to handle the complexities of an elastomeric joint. Finite element analysis can be applied to any field problem with no geometric restrictions as every detail of the geometry can be accurately modeled [44-45]. These codes can examine the complex behavior of rubber which can include quasi-

reversible deformation up to very large strains, hysteresis, Mullins effects, time dependent effects as well as nonlinear or hyper-elastic material behavior [46-48].

4.3 Experiment

To characterize the effect of confinement on a variable thickness elastomeric joint, finite element analysis results from Abaqus (Simulia Inc., Forest Hill, MD) were used to determine stress response for a variety of variable thickness joint geometries. The resulting stresses from the finite element model were compared for the corresponding geometries and then design alternatives were analyzed to try to reduce the stress state and thus improve joint design.

4.3.1) Model Design

Nine different geometries were created and tested to characterize the effect of geometry on the loads seen in the joint. Figure 32 illustrates the basic geometry of the variable thickness joint where the brown region is the elastomeric adhesive and the green is the glass adherend.

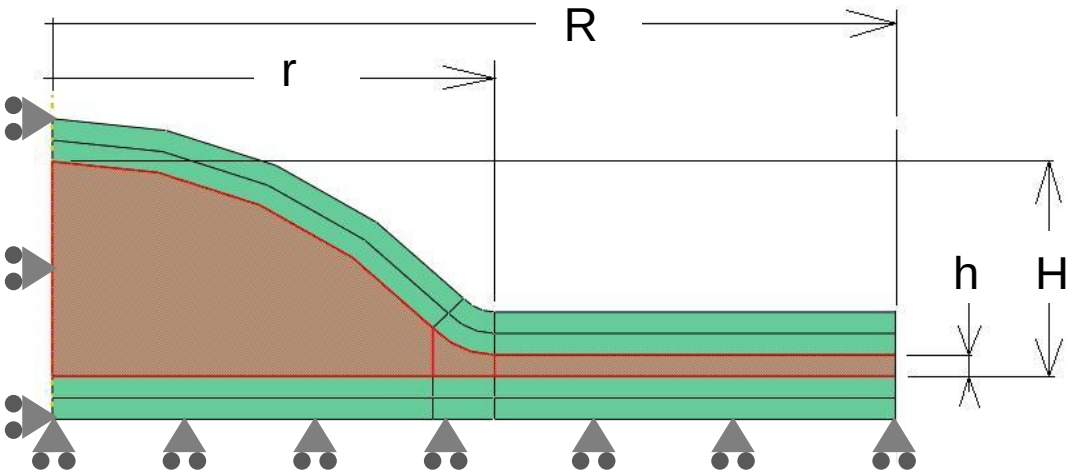

Figure 32: Model geometry for finite element analysis with pinned boundary conditions shown

The model was an axisymmetric deformable part where the axis of symmetry is at the left most edge of the model and is shown as a dashed line in Figure 32. To vary the geometry of the model, r and h are held constant at 100 and 5 mm, respectively. The thickness of the glass is also held to be constant at 10 mm. R and H were modified to observe the effect of increased variable thickness as well as increased land region. These values were modified following the model tree see in Table 2.

Model Tree		H/h		
		2	5	10
R/r	1.2	1	2	3
	2	4	5	6
	5	7	8	9

Table 2: Model tree for varying the joint geometry

Additionally, to observe how varying the thickness of the adhesive in the land region affects the stress state, h was modified for model 9 to 1 mm and 2 mm thickness. To monitor how design recommendations affect the stress state in the joint, two different models have been studied. The effects of a hole in the center of the joint were examined by constructing the model seen in Figure 33.

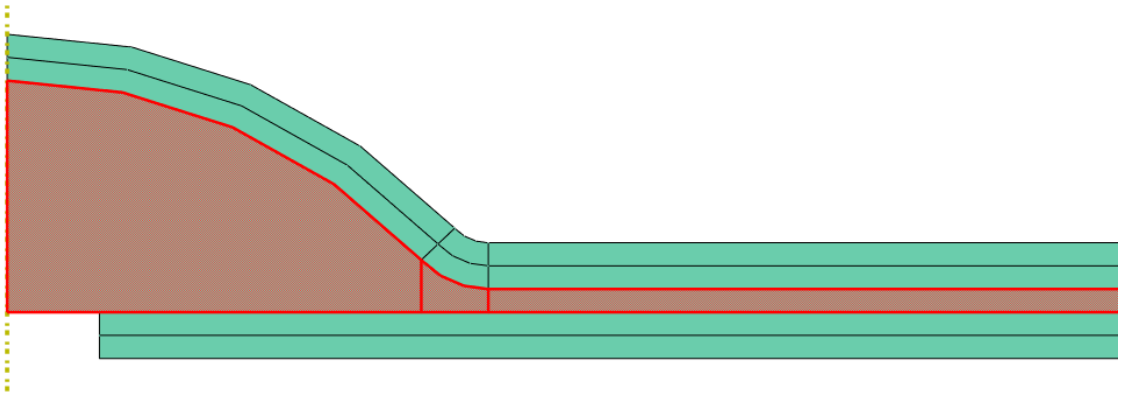

Figure 33: Finite element model with hole

To add to this, the finite element model with a hole free of material was filled with the adhesive as keeping this region free of adhesive could be a practical challenge. To examine these effects, the model seen in Figure 34 was constructed where again the brown region is the elastomeric adhesive and the blue is the glass adherend.

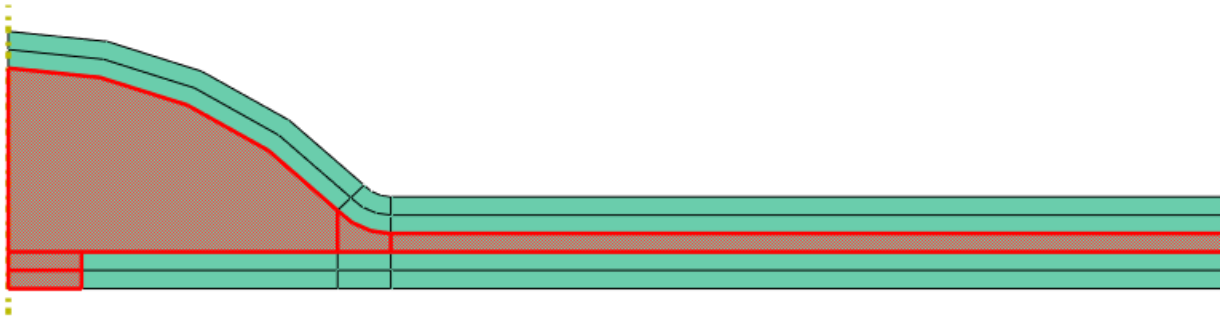

Figure 34: Finite element model with hole filled with adhesive

Additionally, while a challenging feat to conduct in real life, an axisymmetric groove was incorporated into the lower adherend as seen in Figure 35 where the red region is the adhesive and the blue is the glass adherend.

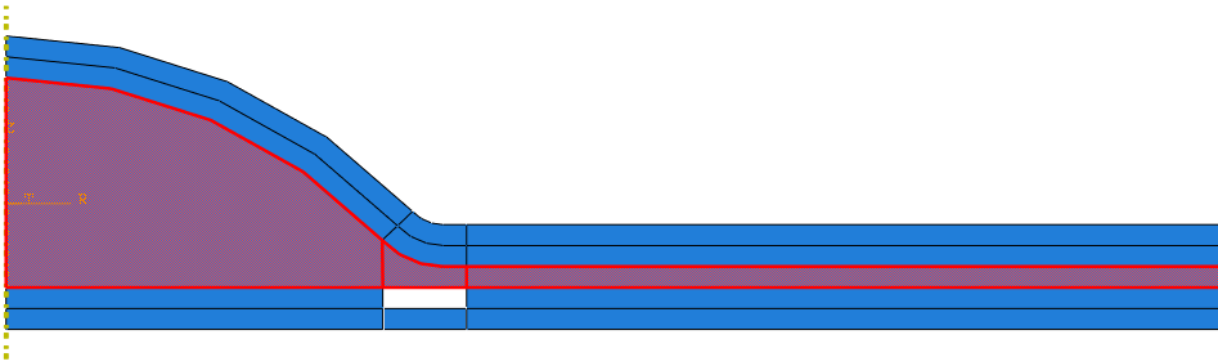

Figure 35: Finite element model with axisymmetric groove

The optimized location of this groove was investigated by changing the location and thickness of the groove. Three different locations were tested which include positions directly below the

transition fillet, 40 mm to the left of this fillet, and 40 mm to the right. Also, three different groove widths (5, 10 and 20 mm) were incorporated in the analysis.

4.3.2) Material model

The material model used in this finite element model was the same for all geometries tested. Both the adhesive and the adherend were considered following a linear elastic behavior. Since this model was constructed for a silicone adhesive with a glass adherend, these materials were used for this investigation. For the glass section, the elastic modulus and Poisson's ratio were 60 GPa and 0.2, respectively. For the adhesive, the modulus and Poisson's ratio were 1 MPa and 0.4995, respectively. Additionally the coefficients for thermal expansion, expressed volumetrically were considered to be 8.5×10^{-6} and 0.002 per degree Celsius for the glass and the adhesive, respectively.

4.3.3) Boundary conditions and loading

Since the intent of the Dreaming project was to display artistic work on the side of a building, the bottom glass panel is mounted to the building and thus the bottom edge of the glass is considered to be pinned on rollers in the radial direction such that the bottom edge is free to move in the radial or R direction but is restricted from moving in the Z or thickness direction. Additionally, since this model is axisymmetric, the left edge of the joint is not allowed to expand in the radial direction. Furthermore, to examine the effects of thermal expansion, the material was subjected to a uniform temperature change of +50 °C.

4.3.4) Meshing

The axisymmetric model was meshed using reduced integration, four-noded quadrilateral element (CAX4R). The mesh was checked for both P-type and H-type convergence, where P-type convergence examines the order of the finite element

approximation and H-type examines the amount of elements used. An example of the meshing distribution for one model can be seen in Figure 36 .

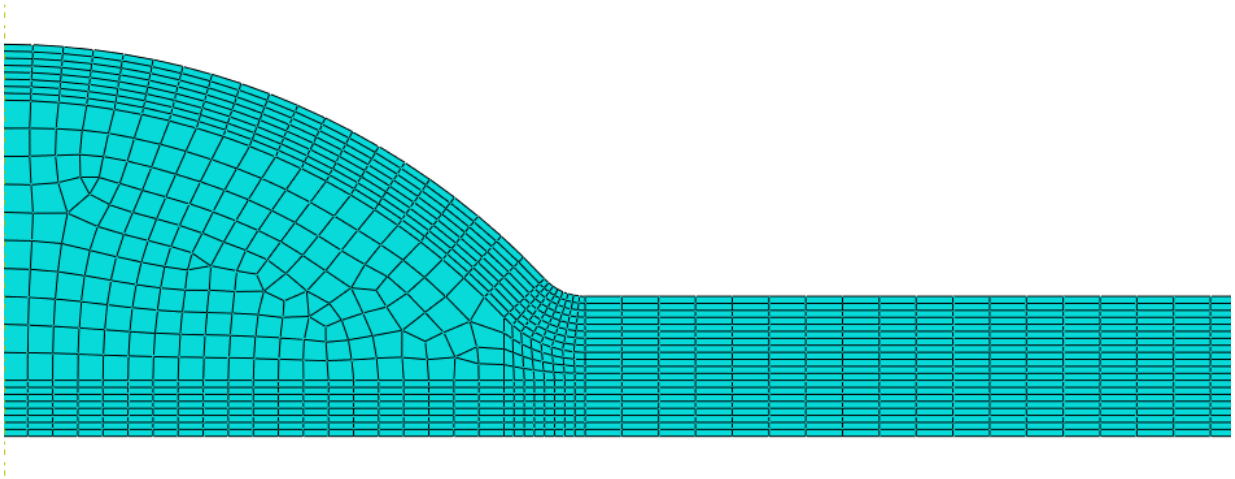

Figure 36: Example of the finite element mesh distribution

For the mesh density tested, which consists of approximately 1500 elements, the mesh was checked for both h and p type convergence. This is done by increasing the number of elements or the order of the polynomial used to represent the displacement field, respectively. Results from the mesh convergence check showed only a 3% difference from the mesh scheme chosen compared to one of higher order and element number suggesting that the mesh chosen can provide a good representation of the actual response.

4.4 Results and Discussions

To investigate the effects of a variable thickness sealant layer, finite element analysis was used to analyze the stresses at the interface, i.e. the elastomeric pressure and the shear as well as the maximum principal and von Mises stress in the glass adherends. The pressure and shear at the interface were measured for each node along the interface of the glass and the adhesive. The maximum principal and von Mises stresses were examined for the adherend only. This was performed to determine the maximal stresses in the adherend. Both were

examined here as each corresponds to different failure criterion, maximum principal stresses would be used to determine failure for a brittle material like glass which is investigated here, whereas von Mises stresses are used to determine yield in ductile materials [49]. Figure 37 illustrates from the Abaqus visualization module the von Mises stresses in model 9 for the entire field.

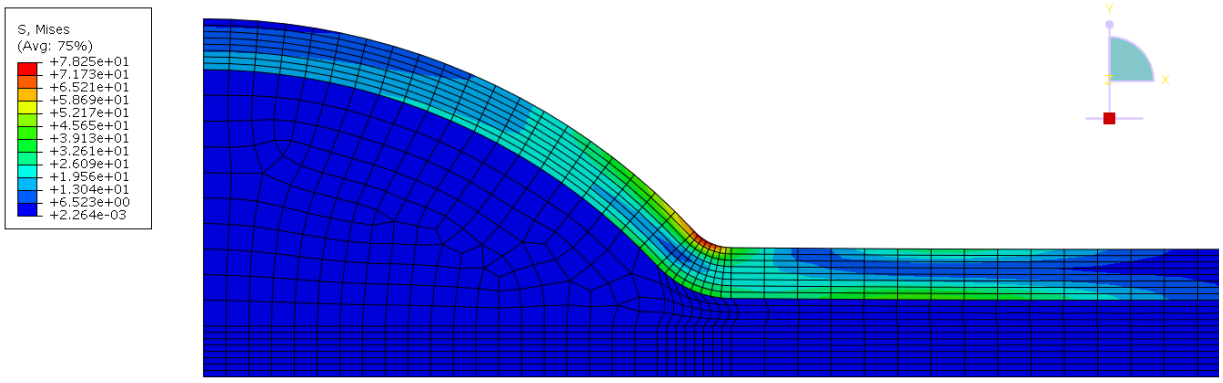

Figure 37: Abaqus Results of Von Mises stress for Model 9

Since the stresses in the glass are much higher than those seen in the elastomer, they are lost in the visualization window. To examine the effects in just the elastomer, the elastomer is examined by itself. The result for the hydrostatic pressure for the joint geometry 9 can be seen in Figure 38.

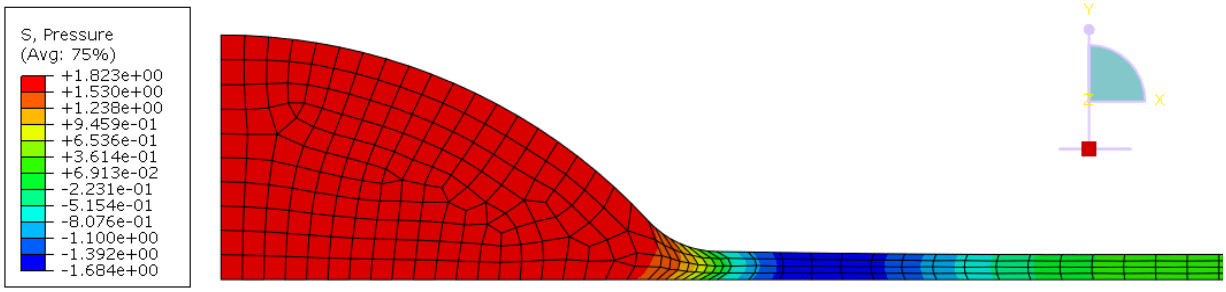

Figure 38: Abaqus Results of hydrostatic pressure on the elastomer in Model 9

It is interesting to note that the pressure in the land region becomes compressive before equilibrating at a steady value of approximately zero.

4.4.1) Effects of Profile Height

To examine the effects of profile height as seen in Figure 39, the region of land (R) is held constant at 200 mm and the height of the bulb is modified.

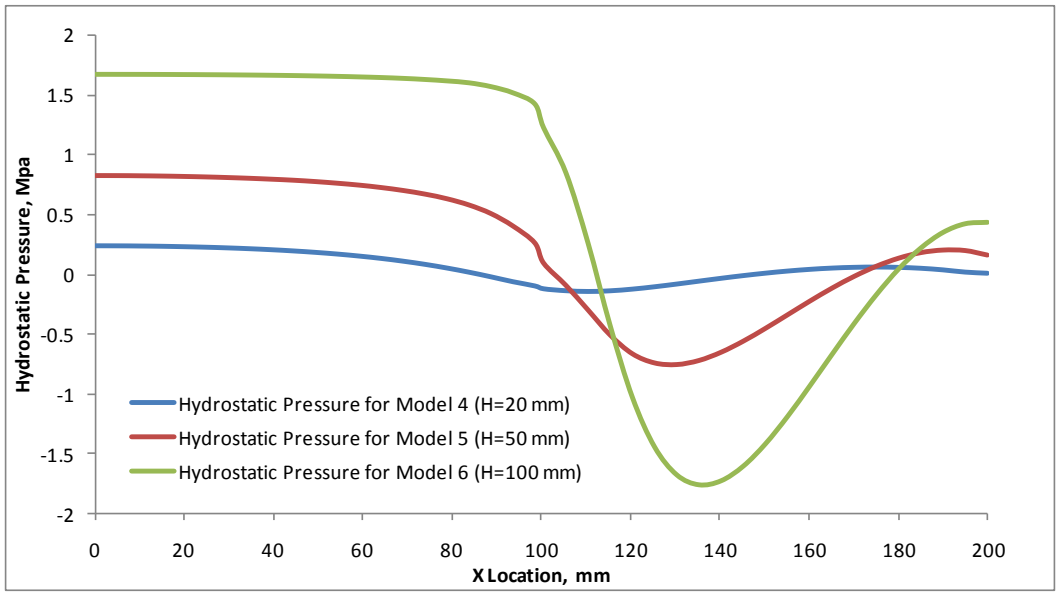

Figure 39: Effects of profile height on hydrostatic pressure at the interface

Models 4, 5 and 6 correspond with profile heights (H) of 20, 50 and 100 mm, respectively. As seen in Figure 39, increasing the profile height (H) greatly effects the pressure on the glass and is assumed to be the dominate mechanism behind the adherend failure. The effects of shear for these models have been investigated seen in Figure 40.

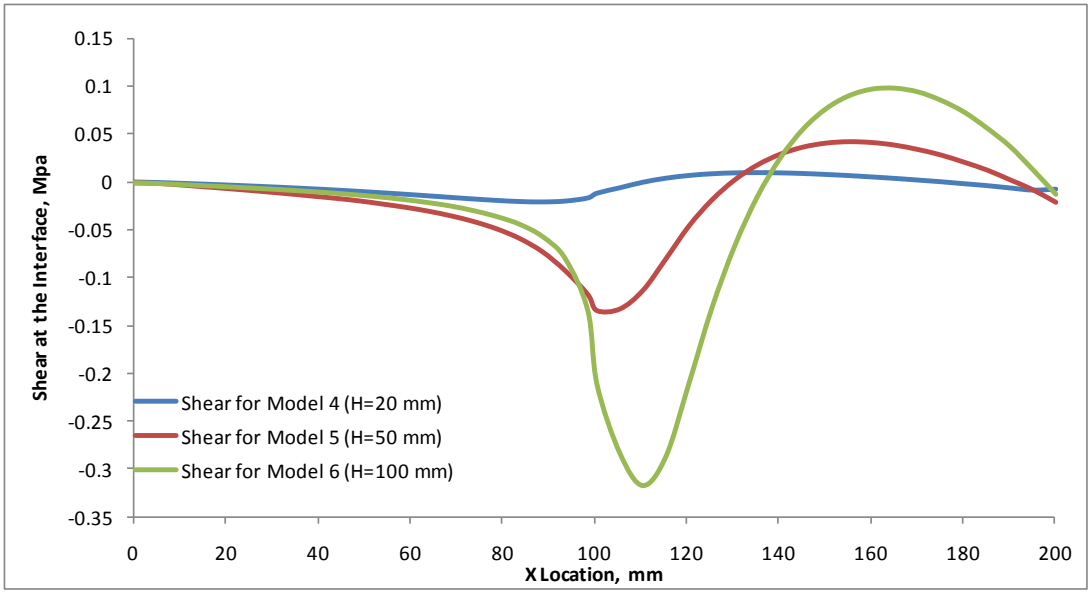

Figure 40: Effects of profile height on shear stress at the interface of the joint

This figure shows that as profile height increases, the shear stresses at the interface increase in response to more material trying to expand but being confined by the rigid adherend. A slight discontinuity can be seen at x=100 mm, this can be attributed to the transition from the variable thickness to the land region. This transition is gradual as a fillet of 10 mm exists in this region however, there a stress singularity may still exist causing a discontinuity in this region. Furthermore, the effects of changing the length of land have been examined in Figure 41.

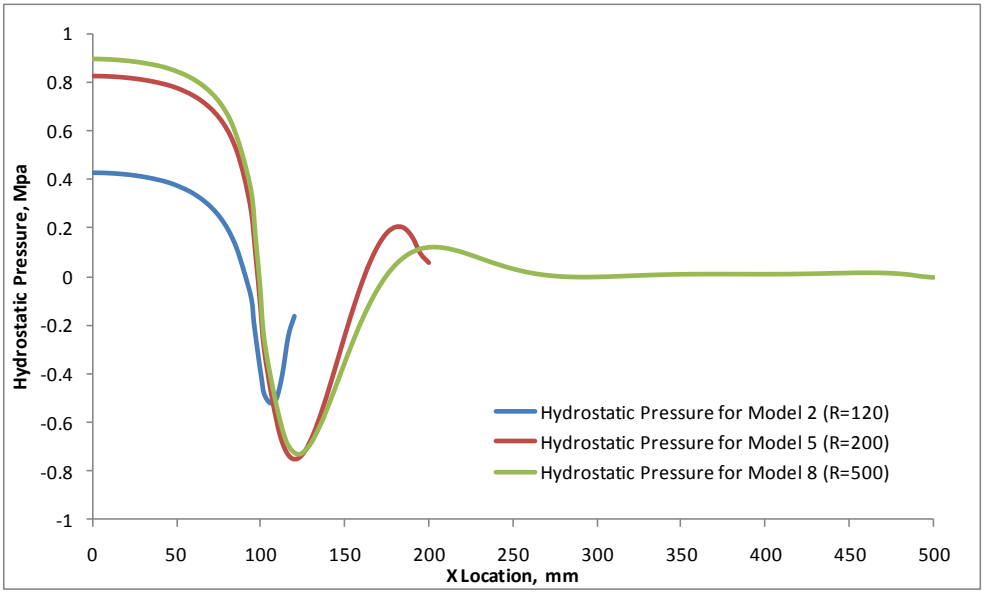

Figure 41: Effects of increased land on hydrostatic pressure at the interface

Models 2, 5 and 8 correspond with a fixed profile height of 50 mm and a land region of 120, 200 and 500 mm, respectively. It is shown that as the confinement on the elastomer in the radial direction increases, the amount of hydrostatic stress at the interface increases. A summary of the maximum hydrostatic and shear stresses at the interface as well as the maximum principal and von Mises stresses in the adherend can be seen in Table 3.

	Maximum Adhesive Pressure	Max Shear in Interface	Maximum Von Mises Stress in the Adherend	Maximum Principal Stress in the Adherend
Model 1	0.18	0.02	10.18	10.17
Model 2	0.43	0.11	12.81	11.52
Model 3	0.59	0.26	18.24	18.04
Model 4	0.24	0.02	11.18	11.79
Model 5	0.83	0.14	21.43	23.91
Model 6	1.67	0.32	72.37	82.87
Model 7	0.26	0.02	11.5	11.47
Model 8	0.90	0.14	23.6	25.96
Model 9	1.82	0.34	78.25	90.71

Table 3: Summary of the maximum stresses seen in the joint over all geometries investigated

Models 1 through 3 have a profile height of 20 mm and a varying land region of 120, 200 and 500 mm respectively. Models 4 through 6 have a constant profile height of 50 mm and a land region of 120, 200 and 500 mm respectively. Models 7-9 have a profile height of 100 mm and a varying land region of 120, 200 and 500 mm respectively. It can be seen from this table that both increasing the land region and profile height has the largest effect on the joint and causes the most stress in the adherend which could result failure.

4.4.2) Effects of varying h

To examine the effect of varying the profile height in the land region, h, model 9 which exhibits the highest principal stresses in the adherend as well as the highest hydrostatic pressure at the interface was modified to include several h values. An examination of the hydrostatic pressure for h varying can be seen in Figure 42.

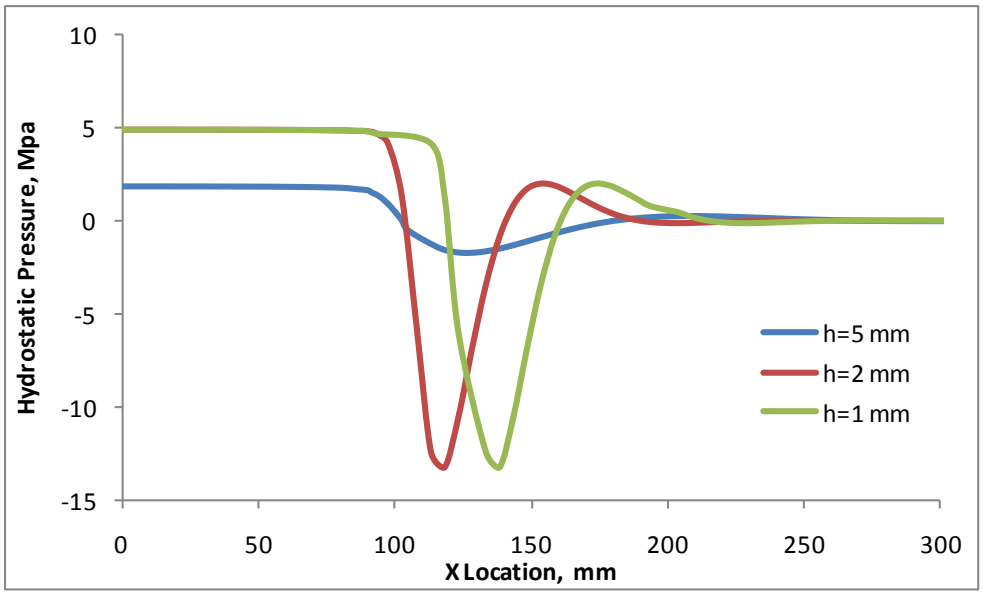

Figure 42: Effects of varying h hydrostatic pressure at the interface for model 9

It can be seen here that decreasing the profile height in the land region causes the hydrostatic pressures to increase 170%. Also it can be seen that varying h from 2 mm to 1 mm seems to not affect the magnitude of the hydrostatic pressure but increases the area of high pressure.

This is an effect of the additional confinement as the elastomer cannot equilibrate the hydrostatic pressure from the variable thickness as h decreases. A summary of the maximum stresses for varying h can be seen in Table 4 .

	Maximum Hydrostatic Pressure (MPa)	Maximum Shear at Interface (MPa)	Maximum Von Mises Stress in the Adherend (MPa)	Maximum Principal Stress in the Adherend (MPa)
Model 9 h=5 mm	1.82	0.34	78.25	90.71
Model 9 h=2 mm	4.91	0.80	117	133
Model 9 h=1 mm	4.91	0.80	111.6	127.9

Table 4: Summary of the maximum stresses for varying h for model 9

It can be seen that, for all cases investigated, decreasing h greatly increases the stress in both the adherend and at the interface.

4.4.3) Effects of design modifications on stress state

In order to investigate the effects of design modifications on a variable thickness joint, model 9 was again modified to incorporate several design changes. The effects of drilling a hole at left most edge was investigated for holes drilled with a radius of 5, 10 and 20 mm. Additionally, the effects were examined for cases in which the hole was free of material or filled with adhesive. A summary of the hydrostatic pressures for these design modifications can be seen in Figure 43.

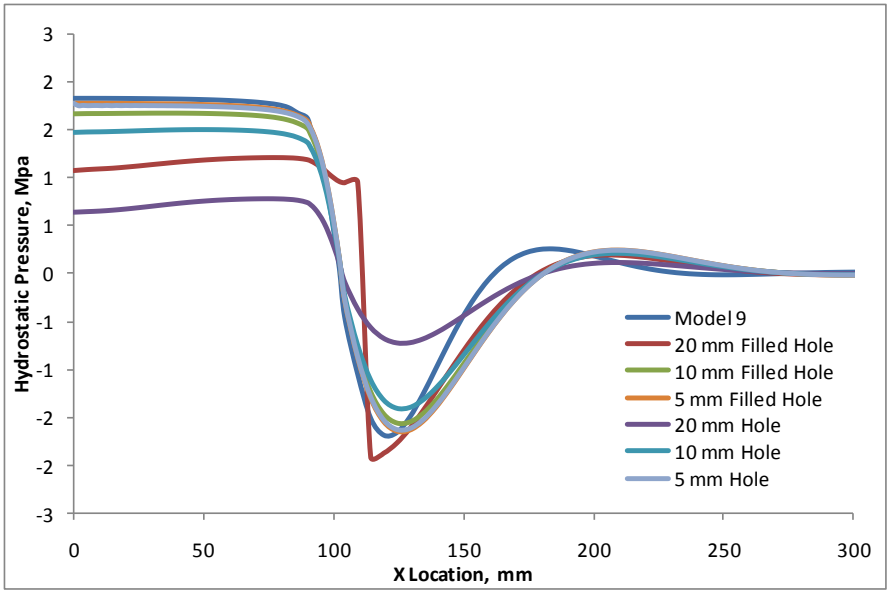

Figure 43: Hydrostatic pressure comparison for design modifications which include a filled and empty hole

As seen above, all models showed a decrease in the hydrostatic pressure. By incorporating a hole of 20 mm free of material, the largest decrease in hydrostatic stress is seen. Also, by including either a filled or empty hole of 5 mm has little effect on the stress state. A summary of these results is illustrated in Table 5 where for all design modifications, except for the small radius filled hole case, a decrease in the stresses at the interface as well as in the adherend is observed.

	Percent Change of Adhesive Pressure	Percent Change of Shear at Interface	Percent Change of Von Mises Stress in the Adherend	Percent Change of Principal Stress in the Adherend
Hole-20	-57.42	-45.92	-56.42	-60.99
Hole-10	-17.49	2.85	-15.67	-15.64
Hole-5	-2.82	18.20	-3.55	-3.47
Filled Hole 20	-45.56	-31.13	-44.01	-43.96
Filled Hole-10	-8.62	13.14	-7.02	-7.00
Filled Hole-5	-2.20	20.18	-1.24	-1.23

Table 5: Summary maximum stresses seen in the joint over for design recommendations which incorporate both a filled and a free hole

Furthermore, an interesting solution examined was the incorporation of an axisymmetric groove with variable width and location of the stress relief zone. This design would be hard to

accomplish, however, an investigation of its effects has been performed. An illustration of the visualization of the groove can be seen in Figure 44 where for this particular model, the groove is 20 mm and at the center of the transition.

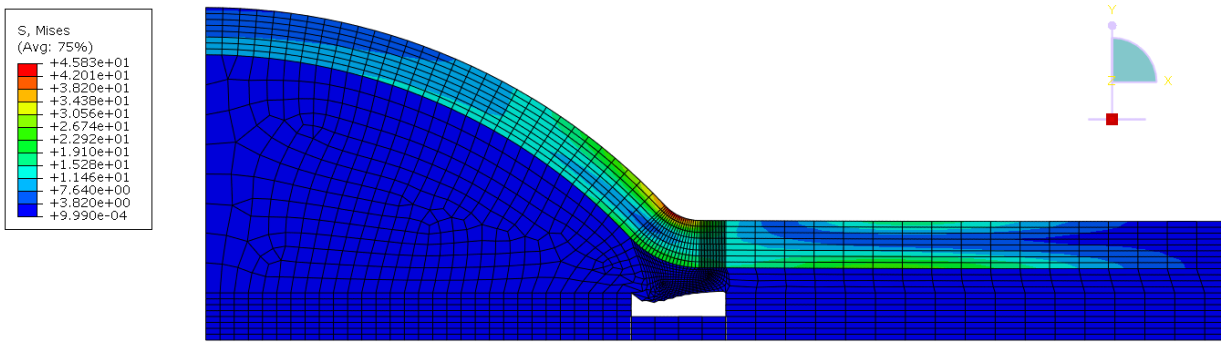

Figure 44: Model 9 with an axisymmetric groove of 20 mm at the center of the transition

It is interesting to note that for all cases except for the grove placed at the right of the transition, an expansion of the adhesive is observed as seen above. For the models which contain a stress release positioned 40 mm to the right of the transition, the adhesive in this region contracts due to thermal expansion. A summary of the hydrostatic pressures for this design alteration can be seen in Figure 45 where the groove width is held constant at 20 mm and the location is changed.

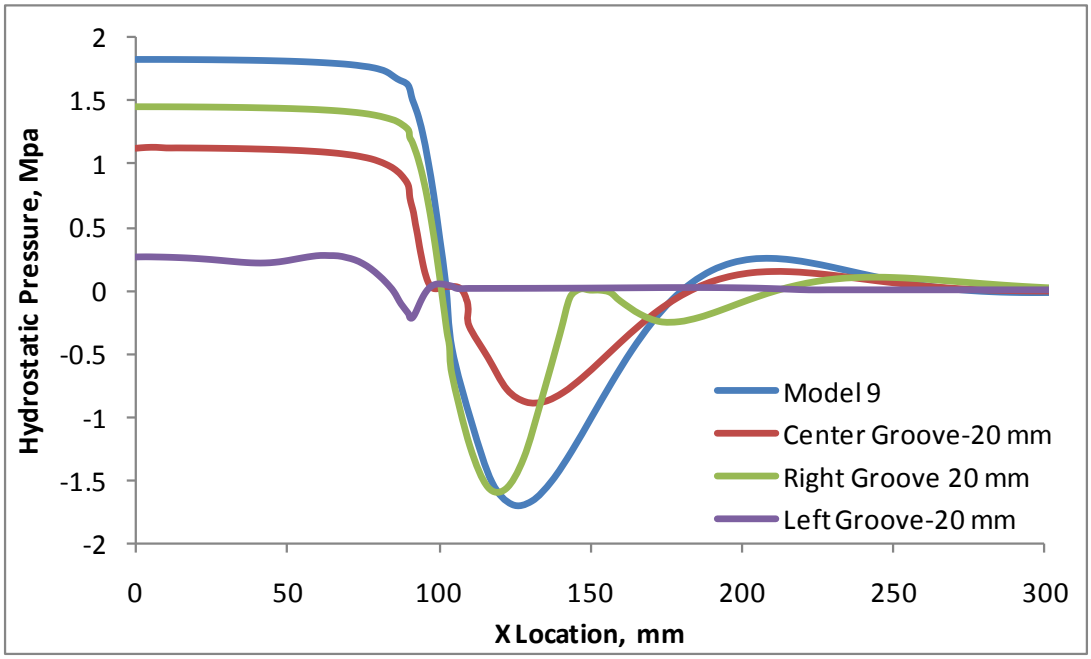

Figure 45: Comparison of the hydrostatic forces for design alterations which incorporate an axisymmetric groove

This graph illustrates that for all models which incorporate a groove, the hydrostatic pressures drop. Additionally, it can be seen that by including this stress relief to the left of the transition the largest decrease in hydrostatic pressure is observed. A summary of the effects of the groove can be seen in Table 6.

	Percent Change of Adhesive Pressure	Percent Change of Shear at Interface	Percent Change of Von Misses Stress in the Adherend	Percent Change of Principal Stress in the Adherend
Left-20	-84.92	-82.02	-85.35	-85.32
Left-10	-60.07	-53.25	-61.57	-61.15
Left-5	-29.60	-29.65	-29.50	-29.49
Center-20	-37.92	-46.06	-41.43	-41.51
Center-10	-32.17	-33.60	-42.47	-42.59
Center-5	-12.52	-6.70	-19.19	-19.36
Right-20	-20.24	15.47	-21.56	-21.66
Right-10	-19.59	13.44	-19.11	-19.12
Right-5	-1.74	12.66	-0.83	-0.84

Table 6: Summary maximum stresses seen in the joint over for a grooved joint

This table illustrates that for all design modifications, the hydrostatic stresses in interface and both the principal and von Mises stresses in the adherend dropped for all cases. Additionally, the shear at the interface is reduced for all models except for the models which incorporate a groove at the right of the transition. While the inclusion of an axisymmetric groove in a brittle sample would be very difficult to achieve it provides the largest reduction in stresses at the interface as well as in the adherend.

4.5 Conclusion

The impact of confinement has been evaluated for a variable thickness joint under thermal expansion using finite element analysis. This effect has been tested for various geometries as well as examined for models whose design has been altered to decrease the impact of thermal expansion of a variable thickness joint. By comparing the results for hydrostatic pressure and shear stress at the interface as well as comparing the principal and von Mises stresses for a variety of geometries, various design options can be evaluated. It was shown that an increase in either the profile height (H) or land region (R) causes the stresses at both the interface and in the adherend to increase. Additionally, by incorporating a hole or an axisymmetric groove, the stresses at the adhesive and at the interface can be dramatically reduced.

Chapter 5: Conclusion

The elastomeric seal used in fuel cell applications is subjected to aggressive environments where temperature and acidic conditions affect the durability of the fuel cell. Any degradation of this material could cause the seal to leak and thus impact performance of this alternative energy solution. To determine the effects of degradation, the momentary and relaxed stiffness has been evaluated for these seals. Additionally, the material's mechanical behavior as well as tearing energy has been examined. In order to simulate a fuel cell environment, all tests have been performed in an aggressive environment. These properties have been evaluated by conducting momentary and relaxed stiffness tests, uniaxial tension, and trouser tear tests. By conducting these experiments, we can determine the materials mechanical response over time and by comparing these results to the as-received material we can determine the durability of the material in an aggressive environment.

By evaluating the momentary and relaxed stiffness, a comparison can be made between rate of additional crosslinking in the presence of chain scissioning and chain scissioning effects alone. From this test it was seen that the momentary stiffness results for samples in liquid environment there was little change in sealing force. This suggests that the rate of chain scissioning is equivalent to that of additional crosslinking or none occurs at all. For momentary stress relaxation for air-aged samples, it was seen that the rate of crosslinking was higher than that of chain scissioning, which can be seen by an increase in momentary stiffness for these samples. Stress relaxation tests, in liquid environment showed 16% decay in load over time. Additionally, these samples illustrate small changes in relaxation after an extended period of time suggesting, that the chemical degradation process has slowed after 2700 hours. Stress relaxation tests in air showed a similar decay where the rate of degradation was higher for 120 °C samples compared to 90 °C.

For the uniaxial tension tests, small decreases in the ultimate properties of the material occur after 2700 hours for strain and aged conditions. However, due to additional crosslinking in the strained states, the secant modulus at 100% strain of the material experiences an increase for all cases.

The tearing energy for this hydrocarbon material has been evaluated using trouser tests. Trouser tests were carried out under various rates, temperatures, and environments to determine the tearing energy as a function of aging. Furthermore, it was observed that this behavior was shown to follow time temperature superposition and was in good agreement with the constitutive data obtained from dynamic mechanical analysis. Results showed that for all aging conditions, the tearing energy of this material has increased for all aging environments. Additionally, fracture tests in environment shows the onset of a threshold value, below which fracture will not occur.

Additional work, unrelated to fuel cell seals, has been performed to examine the impact of confinement for a variable thickness adhesive joint undergoing thermal expansion. The loads in the joint were evaluated using finite element analysis and compared for various geometries. Additionally, the joint design was altered and examined in an attempt to reduce the impact of this variable thickness thermal expansion. The hydrostatic pressure and shear at the interface as well as the maximum von Mises and principal stresses in the adherend were examined to understand the complex effects of joint geometry. Results show that increasing either the profile height or the land causes the stresses at both the interface and in the adherend to increase. Additionally, by changing the design to incorporate stress relief through either a hole or a grove reduced the stresses in the interface for all design alternatives analyzed.

5.1 Future Work

Although significant results were collected from material characterization of an elastomer used for a fuel cell seal more research is needed to fully understand the durability of this material. Additionally, other parameters need to be evaluated to understand the complexities of a variable thickness joint. In order to examine some of these issues the following future work may be carried out.

5.1.1) Momentary and Relaxed Stiffness Examination

While a good deal of testing was carried out to determine the change in momentary and relaxed stiffness as a function of aging for these seals, further investigation is needed to examine the impact of environment. In order to examine the impact of environment, by increasing the concentration of the environments tested in this research, more aggressive testing can be performed. Additionally, increasing the range of temperatures as well as prescribed strains could allow for a more complete understanding of the compressive properties of these seals.

5.1.2) Tensile Properties

Insight into this material's mechanical behavior as a function of aging has been evaluated for a variety of environmental conditions. To expand this research, longer aging times need to be evaluated for this material as current aging times showed little change. Another way to increase the aging time would be to impose a larger strain on the samples.

5.1.3) Tearing Properties

To expand the results from tearing for various rates and aging conditions, tearing predictions could be investigated using finite element analysis. By incorporating the mechanical properties as well as tearing properties into a finite element code, accurate predictions of life can be

evaluated for a variety of loading conditions. Specifically for a fuel cell, thermal and compressive cycling could be evaluated for these seals in an attempt to accurately predict life.

5.1.4) Analysis of a Variable Thickness Joint

Further modeling efforts are needed to completely understand the effects of the joint design which was investigated in this research. The finite element model could be expanded to incorporate fracture at the interface of the joint as well as in the adherend. Additionally, the model could be expanded to incorporate a hyper-elastic temperature dependent material model. Also, cyclic thermal loading could be performed on this advanced model to determine the effects of confinement on joint life.

References

1. Ronan, S., et al., *Long-term stress relaxation prediction for elastomers using the time-temperature superposition method.* Materials & Design, 2007. **28**(5): p. 1513-1523.
2. Gillen, K.T., M.R. Keenan, and J. Wise, *New method for predicting lifetime of seals from compression-stress relaxation experiments.* Die Angewandte Makromolekulare Chemie, 1998. **261-262**(1): p. 83-92.
3. Tan, J., et al., *Chemical and mechanical stability of EPDM in a PEM fuel cell environment.* Polymer Degradation and Stability, 2009. **94**(11): p. 2072-2078.
4. Curro, J.G. and E.A. Salazar, *Physical and chemical stress relaxation of elastomers.* Journal of Applied Polymer Science, 1975. **19**(9): p. 2571-2581.
5. Rottach, D.R., et al., *Effect of Strain History on Stress and Permanent Set in Cross-Linking Networks: A Molecular Dynamics Study.* Macromolecules, 2004. **37**(14): p. 5468-5473.
6. Wineman, A. and J. Shaw, *A Correspondence Principle for Scission-Induced Stress Relaxation in Elastomeric Components.* Journal of Applied Mechanics, 2004. **71**(6): p. 769-773.
7. Pazur, R.J., J. Bielby, and U.D. Bayer, *Continuous compressive stress relaxation of elastomers used in engine sealing applications.* Rubber World, 2004. **229**(5): p. 24-24.
8. Aklonis, J.J., *Introduction to Polymer Viscoelasticity*. 1983, New York: Wiley, Interscience.
9. Andrews, R.D., A.V. Tobolsky, and E.E. Hanson, *The Theory of Permanent Set at Elevated Temperatures in Natural and Synthetic Rubber Vulcanizates.* Journal of Applied Physics, 1946. **17**(5): p. 352-361.
10. Jong, S.R. and T.L. Yu, *Physical aging of poly(ether sulfone)-modified epoxy resin.* Journal of Polymer Science Part B: Polymer Physics, 1997. **35**(1): p. 69-83.
11. Zhou, H., E.A. Lofgren, and S.A. Jabarin, *Effects of microcrystallinity and morphology on physical aging and its associated effects on tensile mechanical and environmental stress cracking properties of poly(ethylene terephthalate).* Journal of Applied Polymer Science, 2009. **112**(5): p. 2906-2917.
12. Bartenev, G.M., *Strength and failure of viscoelastic materials*. 1968: Pergamon.
13. Singh, H.K., *Lifetime Prediction and Durability of Elastomeric Seals for Fuel Cell Applications*, in *Engineering Mechanics*. 2009, Virginia Polytechnic Institue and State University: Blacksburg. p. 223.
14. Gillen, et al., *Methods for predicting more confident lifetimes of seals in air environments*. Vol. 73. 2000, Akron, OH, ETATS-UNIS: American Chemical Society.
15. Brinson, H.F. and L.C. Brinson, *Polymer Engineering Science and Viscoelasticity*. 2008.
16. Wang, J.Z., et al., *Physical aging behavior of high-performance composites.* Composites Science and Technology, 1995. **54**(4): p. 405-415.
17. Croll, S.G., X. Shi, and B.M.D. Fernando, *The interplay of physical aging and degradation during weathering for two crosslinked coatings.* Progress in Organic Coatings, 2008. **61**(2-4): p. 136-144.
18. Aglan, H., M. Calhoun, and L. Allie, *Effect of UV and hygrothermal aging on the mechanical performance of polyurethane elastomers.* Journal of Applied Polymer Science, 2008. **108**(1): p. 558-564.
19. Andrews, E.H., *Fracture in Polymers*. 1968, New York: American Elsevier.
20. Thomas, A.G., *Rupture of rubber.* Rheologica Acta, 1962. **2**(1): p. 63-66.
21. Rivlin, R.S. and A.G. Thomas, *Rupture of rubber. I. Characteristic energy for tearing.* Journal of Polymer Science, 1953. **10**(3): p. 291-318.
22. Griffith, A.A. *The Phenomena of Rupture and Flow in Solids*. 1921; Available from: http://adsabs.harvard.edu/abs/1921RSPTA.221..163G.

23. Sawyers, K.N. and R.S. Rivlin, *The trousers test for rupture.* Engineering Fracture Mechanics, 1974. **6**(3): p. 557-562.
24. Peppas, N.A., *Tear propagation resistance of semicrystalline polymeric networks.* Polymer, 1977. **18**(4): p. 403-407.
25. Anh, T. and T. Vu-Khanh, *Effects of thermal aging on fracture performance of polychloroprene.* Journal of Materials Science, 2005. **40**(19): p. 5243-5248.
26. Bhowmick, A., *Tear strength of elastomers over a range of rates, temperatures and crosslinking: tearing energy spectra.* Journal of Materials Science, 1986. **21**(11): p. 3927-3932.
27. Gdoutos, E.E., P.M. Schubel, and I.M. Daniel, *Determination of Critical Tearing Energy of Tyre Rubber.* Strain, 2004. **40**(3): p. 119-125.
28. Nah, C., et al., *Adhesion strength and fracture behavior between carbon black-filled rubber sheets.* Journal of Adhesion Science & Technology, 2001. **15**(5): p. 583-598.
29. Gent, A.N.a.H., A.W., *On the tear strength of rubbers.* Proc. Int. Rubber Conf., 1968: p. 193-204.
30. Webb, T.W. and E.C. Aifantis, *Loading rate dependence of stick-slip fracture in polymers.* Mechanics Research Communications. **24**(2): p. 115-121.
31. Gent, A.N. and R.H. Tobias, *Threshold tear strength of elastomers.* Journal of Polymer Science: Polymer Physics Edition, 1982. **20**(11): p. 2051-2058.
32. Loha, P., A.K. Bhowmick, and S.N. Chakravarty, *Modification of the peel test for testing of rubber-to-rubber joints.* Polymer Testing, 1987. **7**(3): p. 153-163.
33. White, C., *Predicting the In-Service Performance of Sealant: A Surprisingly Complicated Problem*. 2010, NIST: Gaithersburg, MD.
34. Dillard, D.A., *Fracture and Debonding Assessment of The Dreaming*. 2007, Adhesion Mechanics, LLC: Blacksburg.
35. Gent, A.N. and O.H. Yeoh, *Failure loads for model adhesive joints subjected to tension, compression or torsion.* Journal of Materials Science, 1982. **17**(6): p. 1713-1722.
36. Jeandrau, J.P., *Analysis and design data for adhesively bonded joints.* International Journal of Adhesion and Adhesives, 1991. **11**(2): p. 71-79.
37. Vrana, M.A., *Development of a fracture mechanics based methodology for assessing adhesive bond durability.* Polymeric materials : science and engineering, proceedings of the ACS Division of Polymeric Materials, Science and Engineering, 1992. **67**: p. 45.
38. Dillard, D.A., *Bending of Plates on Thin Elastomeric Foundations.* Journal of Applied Mechanics, 1989. **56**(2): p. 382-386.
39. Gent, A.N., *Friction and wear of highly-elastic solids.* Wear, 1974. **29**(1): p. 111-116.
40. Corson, T.A., *Peel stress distributions between adherends with varying curvature mismatch.* The Journal of Adhesion, 1990. **33**(1): p. 107.
41. Gent, A.N. and E.A. Meinecke, *Compression, bending, and shear of bonded rubber blocks.* Polymer Engineering & Science, 1970. **10**(1): p. 48-53.
42. Gent, A.N., T.Y.P. Chang, and M.B. Leung, *Fracture and fatigue of bonded rubber blocks under compression.* Engineering Fracture Mechanics, 1993. **44**(6): p. 843-855.
43. Chang, Y.W., A.N. Gent, and J. Padovan, *Expansion of a cavity in a rubber block under unequal stresses.* International Journal of Fracture, 1993. **60**(3): p. 283-291.
44. Cook, R.D., et al., *Concepts and Applications of Finite Element Analysis, 4th Edition*. 2001: Wiley.
45. Abdel Wahab, M.M., et al., *Evaluation of Fatigue Damage in Adhesive Bonding: Part 2: Single Lap Joint.* Journal of Adhesion Science and Technology, 2010. **24**: p. 325-345.
46. Moreau, C., *Mechanical behavior of a slightly compressible rubber-like material: Correlation of simulations and experiments.* Rubber Chemistry andTechnology, 1999. **72**(2): p. 269-282.

47. Da Silva, L.F.M., R.F.T. Lima, and R.M.S. Teixeira, *Development of a Computer Program for the Design of Adhesive Joints.* Journal of Adhesion, 2009. **85**(12): p. 889-918.
48. de Morais, A.B., et al., *Strength of epoxy adhesive-bonded stainless-steel joints.* International Journal of Adhesion and Adhesives, 2007. **27**(8): p. 679-686.
49. Dowling, N.E., *Mechanical Behavior of Materials*. 2006: Prentice Hall.